BIOSOURCED POLYMERS: PROCESS DESIGN FOR THE LARGE-SCALE PRODUCTION OF POLY-4-HYDROXYBUTYRATE

A Research Paper submitted to the Department of Chemical Engineering
In Partial Fulfillment of the Requirements for the Degree
Bachelor of Science in Chemical Engineering

Lia Macera

Xhesika Sula

Joseph Bledsoe

By

Christopher J Hall

April 23rd, 2021

ADVISOR
Eric W Anderson, Department of Chemical Engineering

Table of Contents

1. EXECUTIVE SUMMARY 3

2. PROJECT MOTIVATION 4

3. FINAL PRODUCT SPECIFICATIONS 6

3.1. Quality Assurance 7

4. PROCESS FLOW DIAGRAM 8

5. BATCH SCHEDULES 10

6. UPSTREAM PROCESSING 11

6.1. Seed Train 12
6.2. Bioreactor 15
6.3 Mixing Tanks for Feedstocks 23

7. DOWNSTREAM PROCESSES 25

7.1. Centrifugation 26
7.2. Homogenization 28
7.3. Mixing 29
7.4. Filtration 31
7.5. Drying 35
7.6. Extrusion 37
7.7. Sterilization 41

8. ANCILLARY EQUIPEMENT DESIGN 42

8.1. Pumps 42

9. ECONOMICS 46

9.1. Major Equipment Costs 46
9.2. Total Plant Capital Costs 47
9.3. Operational Costs 48
9.3.1. Electricity 49
9.3.2. Sterilization Costs 49
9.3.3. Raw Materials Costs 50
9.3.4. Labor Costs 51
9.4. Anticipated Revenue 52
9.5. Return on Investment Analysis 53

10. ENVIRONMENTAL CONCERNS 55

11. SAFETY CONCERNS 55

12. SOCIETAL IMPACT 56

13. RECOMMENDATIONS AND CONCLUSIONS 57

14. ACKNOWLEDGEMENTS 59

15. APPENDIX A – STREAM TABLE 60

16. APPENDIX B- NOMENCLATURE 61

17. WORKS CITED 64

1. EXECUTIVE SUMMARY

This report details a commercial scale production plant for poly-4-hydroxybutyrate (P4HB) for medical applications such as scaffolding and sutures. The yearly production scale of the biocompatible polymer is 2,700 tons. Twelve 15,000L bioreactors are scheduled such that six of the tanks are harvested post-fermentation each day in order to create a continuous stream of product to be processed in one single series of downstream processing equipment. After fermentation, the bacterial cells containing the biopolymer as inclusion bodies are disrupted and separated from the cell debris and broth mixture using a centrifuge, high pressure homogenizer, and depth filtration unit. The remaining water is removed from the bioplastic slurry before melting and extruding the polymer into sheets to be sent off for ethylene oxide sterilization by a third-party partner.

The direct fixed capital costs are estimated to be approximately $47 million. The total yearly operational costs including materials, utilities, and labor are estimated to be $5.9 million. With a total gross revenue of $18.4 million from sale of the produced P4HB, this results in a gross annual profit of $12.4 million. Assuming a 2-year construction period, 20-year plant life, and a 6% discount rate for the projected value of the plant's investment, a net present value of $55.2 million is to be expected at an internal rate of return of 17.6%. Based on this analysis, our team recommends pursuing this investment and further researching into the design of the proposed biopolymer plant.

2. PROJECT MOTIVATION

The production of P4HB at an industrial scale is performed through a transgenic fermentation process in the bacteria, *E. coli*, a microorganism that has become a dependable, long standing asset to the biopharmaceutical industry (Lin et al., 2015). Tepha, Inc. is the leading producer of P4HB since 2007. The unique biologic and mechanical properties of the Tepha PHA polymers are recognized by an expanding list of corporate partners that now includes Aesculap AG, ENTrigue Surgical, HemCon Medical Technologies, LifeCell Corporation, NMT Medical, and Tornier, Inc (www.Tepha.com). Due to the stereospecificity of the biosynthetic enzymes, the monomeric units are in D – (–) configuration, which is essential for biodegradability and biocompatibility of PHAs. More than 100 different monomers have been reported as PHA constituents, but only a few were produced in amounts high enough to enable the characterization of their properties and development of potential applications (Reis, M. et al., 2013). Growing P4HB through fermentation allows for high yields and additional options for tailoring properties by incorporating other co-monomers and the ability to vary molecular weight (Martin & Williams, 2003).

P4HB is a thermoplastic, linear polyester, produced by recombinant fermentation process rather than through chemical syntheses (Martin & Williams, 2003). The extremely high elasticity of poly-4-hydroxybutyrate (P4HB), comparable to ultrahigh molecular weight polyethylene, is one of the most useful features of P4HB. P4HB has a one of the lowest glass transition temperatures (T_g), similar to polycaprolactone (PCL). Unlike other resorbable polymers, P4HB is exclusively synthesized in fermentation processes. After 10

years of clinical trials, P4HB is unique among all types of PHA produced to date, as the only PHA-based material with FDA clearances for clinical usage starting with an approval for suture applicable in general soft tissue approximation (Utsunomia et al., 2020). P4HB polyester is naturally produced inside cells as storage granules which regulate energy metabolism that does not contain residual metal catalysts that can produce unwanted side effects, such as inflammation. Given the fact that P4HB is biodegradable and yields 4-hydroxybutyrate (4-HB), P4HB is the only PHA approved by the FDA for medical applications (Utsunomia et al., 2020).

The motivation behind our project is to take advantage of the properties of P4HB such as increased flexibility, a moderate resorption rate, and completely neutral degradation biocompatibility. With an ever-increasing market for PHA's needed for medical devices sourced from gram-negative bacteria, the anticipated demand will exceed 60 million pounds per year by 2025 (Misra et al., 2018). This high demand makes it more likely that all P4HB which can be produced will be purchased.

3. FINAL PRODUCT SPECIFICATIONS

The final product being produced is P4HB, a homopolymer of 4-hydroxybutyrate, and is shown in Figure 3.1. The molecular weight of the polymer can be controlled by controlling the enzymes in the engineered pathway, providing P4HB molecular weight up to approximately one million with polydispersity of 2–3 (Martin & Williams, 2003).

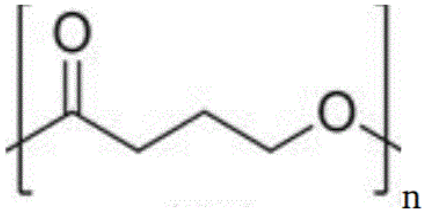

Figure 3.1: Chemical Structure of P4HB

The H-NMR spectrum of purified P4HB will show three characteristic peaks consistent with the structure of the polymer: (1H-NMR (400 MHz, CDCl3) δ = 1.94 (*m*, 2H), 2.37 (*t*, 2H, *J* = 7.4 Hz), 4.10 (*t*, 2H, *J* = 6.6 Hz). The average molecular weight of P4HB is 400-600 kDa, which can be measured by gel permeation chromatography (GPC), in chloroform, relative to polystyrene standards of narrow polydispersity. A Limulus amebocyte lysate assay will be used to measure the bacterial endotoxin content within the purified polymer, ensuring the final product does not contain over the 2 ppm threshold set by the United States Pharmacopeia Convention (U.S. Department of Health and Human Services, 2015). The physical properties of P4HB are shown in Table 3.1.

Table 3.1. Physical Properties of P4HB

T_m (C°)	T_g (C°)	Tensile Strength (MPa)	Cp (J/mol*K)	Form	MW (g/mol)	ΔH_f (kJ/kg)
60	-51	50	1.59	Semicrystalline	86.09	76

3.1. Quality Assurance

The tensile properties of sterile monofilament fibers from multiple lots were determined using a universal mechanical tester according to procedures described in the US Pharmacopeia (USP) standard for testing tensile properties of surgical sutures, which are summarized in Table 3.1.1 (U.S. Department of Health and Human Services, 2015). These tests will be conducted with an Instron 3535 universal testing machine, which is equipped with pneumatic fiber grips, a standard gauge length of 200 nm and a strain rate of 300 mm/minute. Any sample in which breaks occur at the grip, the specimen will be rejected.

Using the European Pharmacopeia procedures, the values of straight tensile strength (LPTS), elongation-to-break, knot pull tensile strength (KPTS), and Young's modulus were determined, and shown below in Table 3.1.1. The Young's modulus quantifies the relationship between tensile stress and axial strain, where the lower the modulus, the less stress is needed to create the same amount of strain. The Frank 56585 bending stiffness test device applies a speed of determination, $6\ ^{0}/s$, with a two second holding time, a maximum angle of 30^{0}, a force of one mN, and a measuring length of 1.0 mm.

Table 3.1.1. Quality Assurance standards for medical grade P4HB

Diameter (mm)	LPTS (N)	KPTS (N)	Bending Stiffness (Pa)	Young's Modulus (GPa)
0.517 ± 0.007	118 ± 6	74 ± 3.1	363 ±7	0.485 ± 0.01

4. PROCESS FLOW DIAGRAM

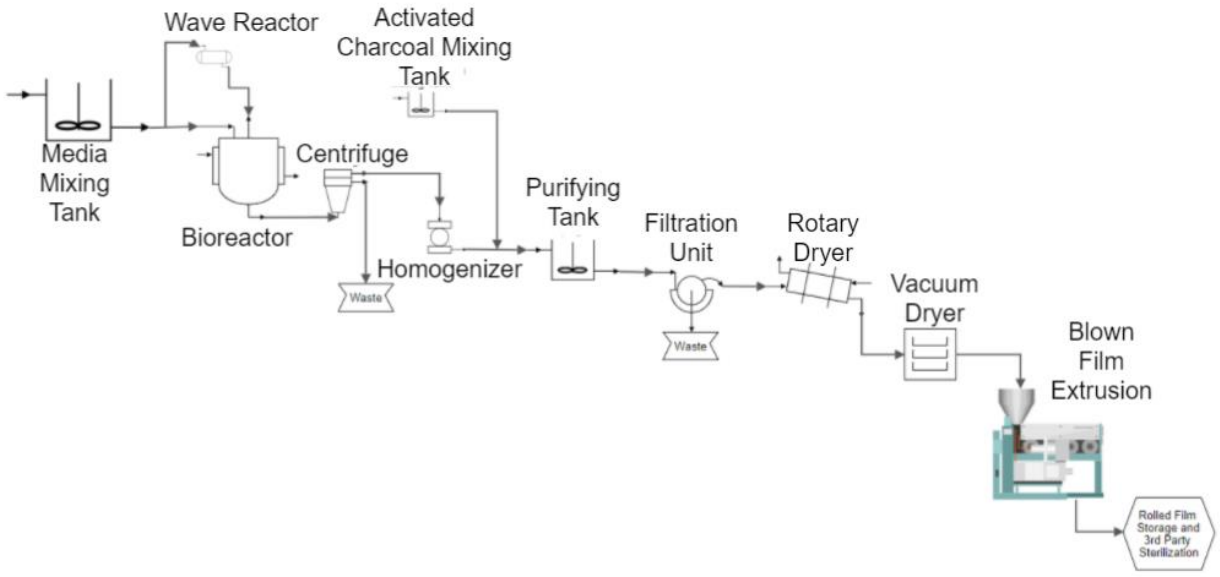

Figure 4.1 Process Flow Diagram where the Wave Reactor and Bioreactor have twelve units, with six finishing each day and Vacuum Dryer has two units

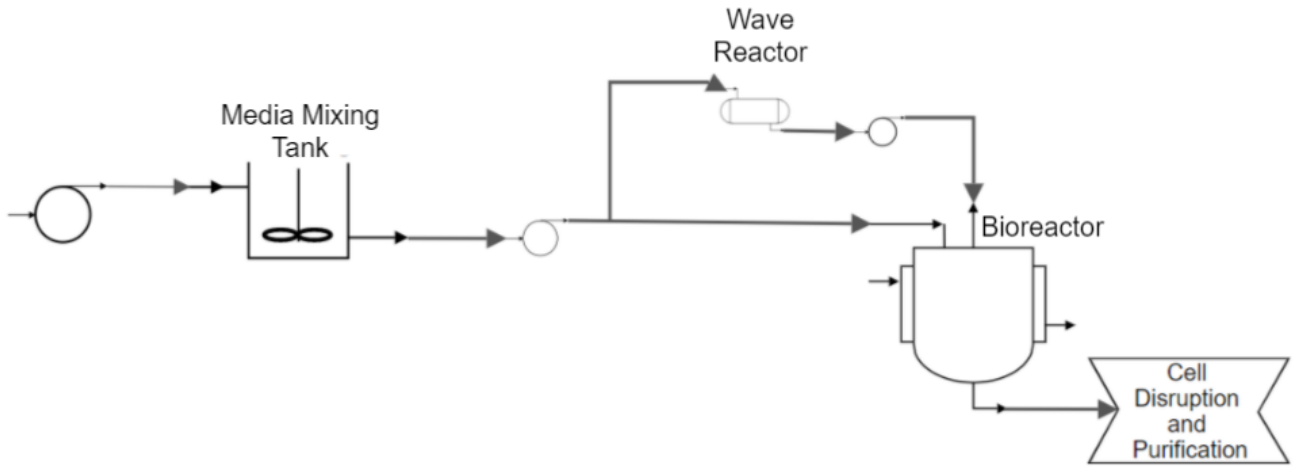

Figure 4.2: Detailed upstream process flow diagram with centrifugal pumps

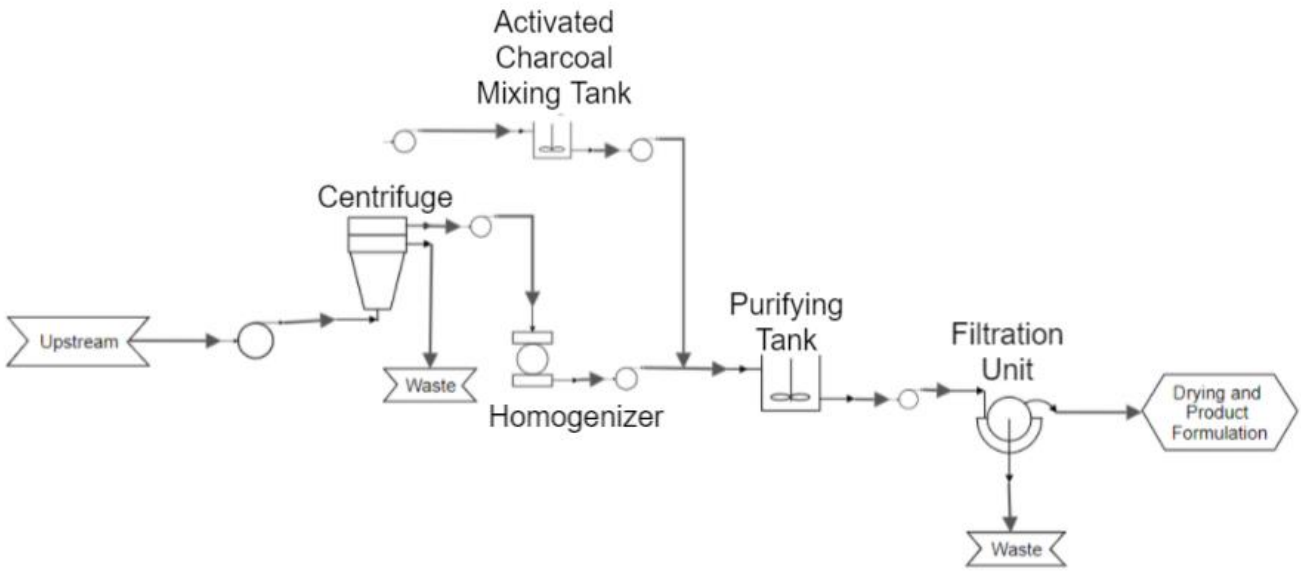

Figure 4.3. Detailed cell disruption and purification process flow diagram with centrifugal pumps

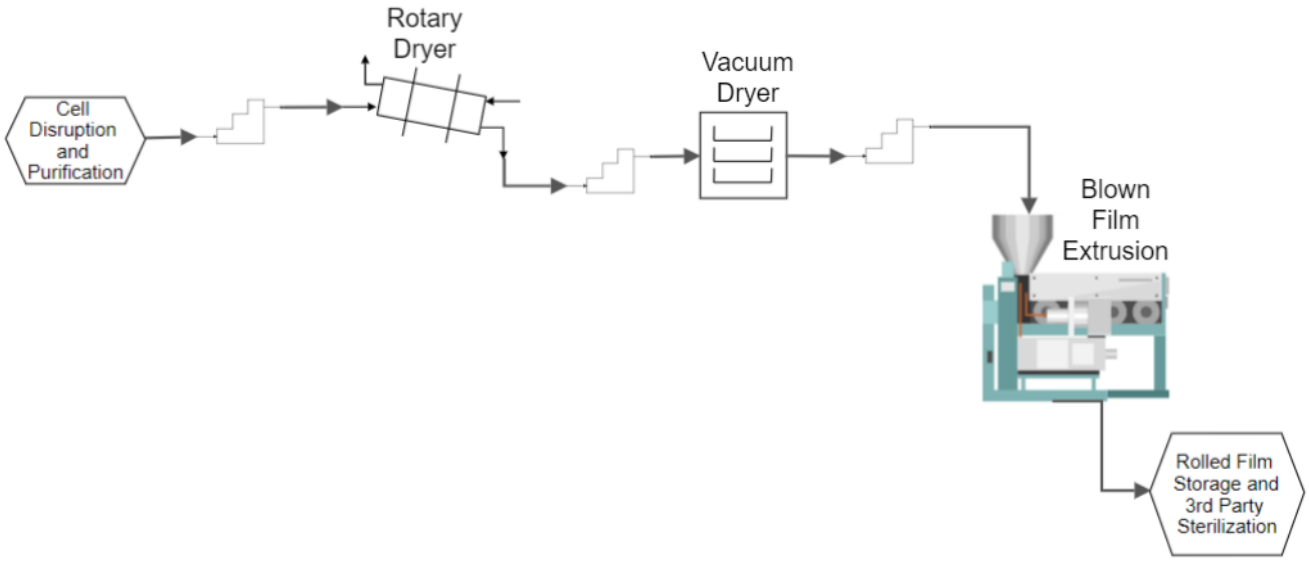

Figure 4.4: Detailed drying and product formation process flow diagram with ancillary equipment

5. BATCH SCHEDULES

The seed train and bioreactor processes each operate on a 36-hour cycle and will consist of two sets of six units working in tandem such that six tanks can be harvested and refed every other day. The purification steps take a total of seven hours, allowing them to be used at the same time to perform the same functions every day with time to clean and replenish stocks between uses. Scheduling allows for a single rotary dryer; however, it will require two vacuum dryers due to the long drying cycles. A summary of the time it takes to complete each task is shown below in Figure 5.1.

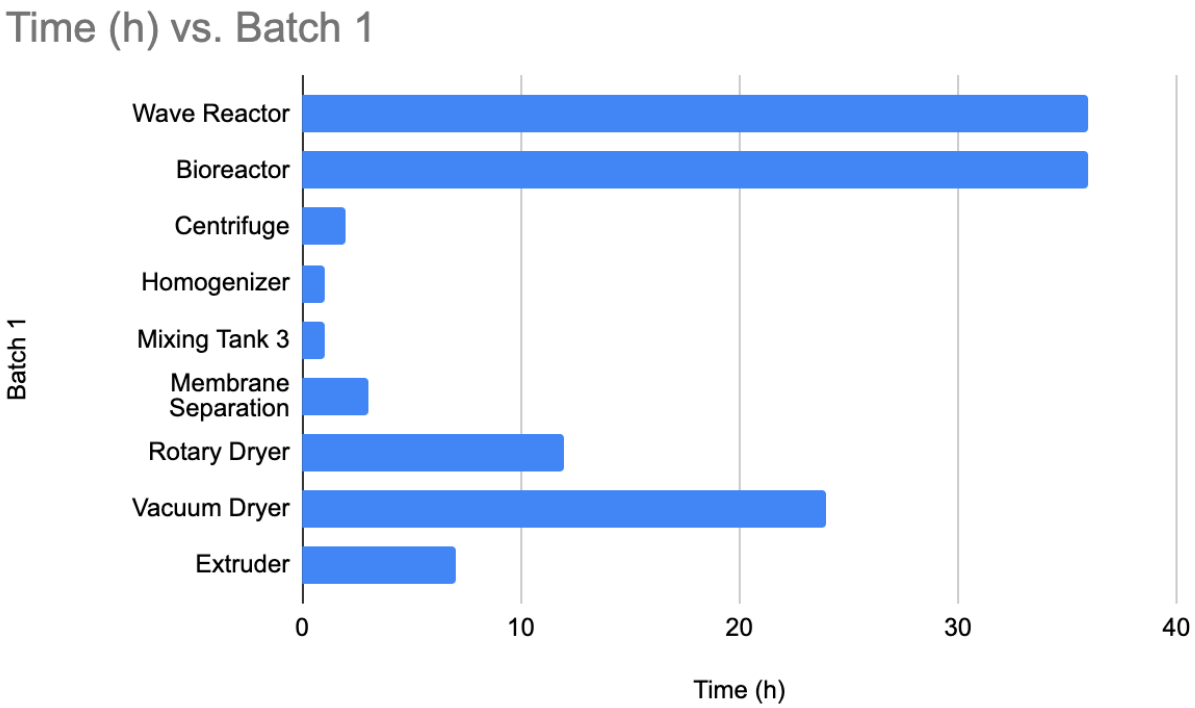

Figure 5.1: Time to complete each unit operation. Wave Reactor and Bioreactor consist of 12 units working in two groups of six, harvested and refed on alternating days. Vacuum dryer consists of two units.

6. UPSTREAM PROCESSING

During the fermentation process, P4HB accumulates inside the fermented cells as distinct granules, making it easily extracted from the cells in a highly pure form. A P4HB content of up to 70 wt % was achieved in a single stage batch culture of the *E. Coli* JM109 Strain (Le Meur et al., 2014). The genetically engineered JM109 microorganism incorporated new biosynthetic pathways to produce P4HB. The JM109 strain is recombination- and endonuclease-deficient, used for routine cloning and plasmid maintenance with no inherent resistance (Agilent.com). *E. coli* was chosen due to its ease of lysing and fast growth rate at high temperatures, allowance for rapid PHA accumulation, and reduction in purification costs (C. Reddy et al., 2003).

6.1. Seed Train

The first step in the design process is to grow the high-density cell stocks in a wave reactor, where a disposable cellbag is filled with gas, cell culture medium, and inoculated cells. The rocker system was chosen over other seed train options as it allows for the

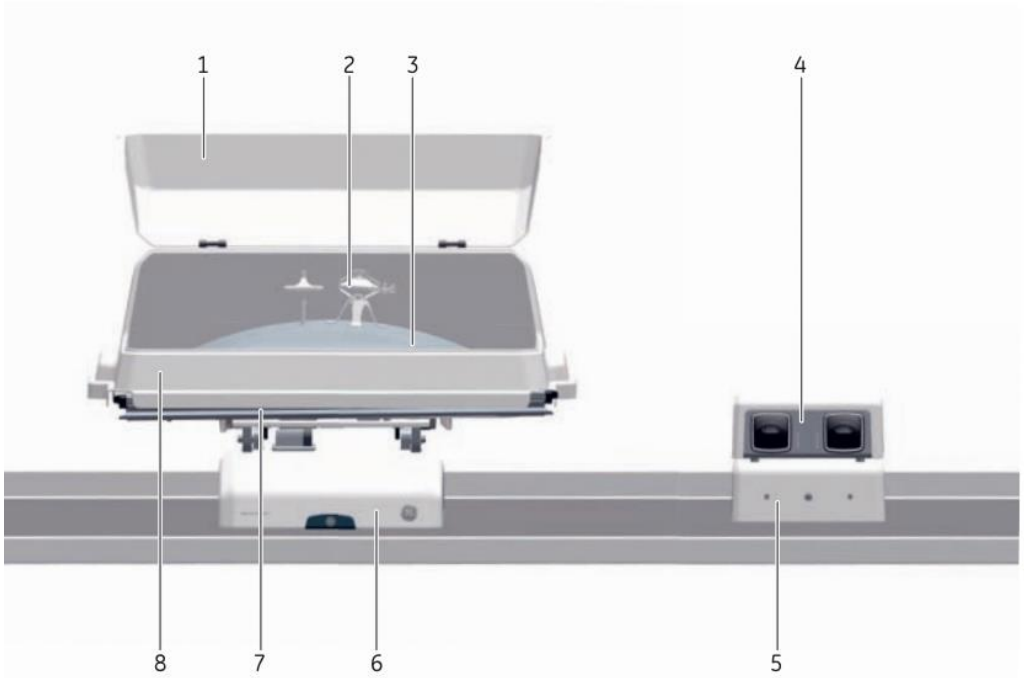

Figure 6.1.1: Wave Bioreactor Illustration. (1) Hatch; (2) Filter Heater; (3) Cellbag Bioreactor; (4) Pump; (5) Process Control Unit; (6) Wave Rocker; (7) Tray; (8) Lid (GE Healthcare)

working volume to be expanded up to ten times in a single cultivation. Main components of the wave bioreactor are shown in Figure 6.1 (GE Healthcare, 2021). The rocker is main unit of the system, through which temperature, rocking speed, rocking angle, and rocking motion are controlled. Each unit has a cellbag in which the bioreaction occurs, a process control unit, the rocker, and the tray and lid. Each cellbag is equipped with a pH sensor port, an outlet gas pressure control valve, inlet and outlet gas filters, a dissolved oxygen sensor port, a sampling port, a port for monitoring optic density, and a cellbag rod to affix the bag to the tray. To maximize efficiency, the *E. coli* strain will be stored in high cell density replenishable glycerol stocks, consisting of 4.5mL of a 50% glycerol solution and

1500 mL of the K.12 *E. coli* cell culture. An embedded computer chip connects the unit to the networked computer. Additional control parameters which impacted the design of this unit operation include gas flow rate, media distribution, pH, oxygen concentration, and desired oxygen concentration regulation. These parameters can be set through the built-in process control unit. The oxygen level is monitored by a plug-in controller to ensure proper saturation. The seed train embedded UNICORN 6.3.2 software which allows for ethernet connections between the computer and instruments. An illustration of the wave reactor is shown below in Figure 6.1.2. Stream 1 is where gas flows into the cellbag bioreactor through the inlet gas filter. Stream 2, shown exiting the reactor, is the metabolic gas waste being expunged through an outlet gas filter. The heated outlet filter prevents clogging and condensation of outlet gas. Stage 3 is depicting the rocking mechanism which sets the rocking platform in motion. The rocking motion, shown as (4) in Figure 6.1.2, allows for continuous and cautious mixing and optimal gas transfer rates. Operational settings for the Wave 25

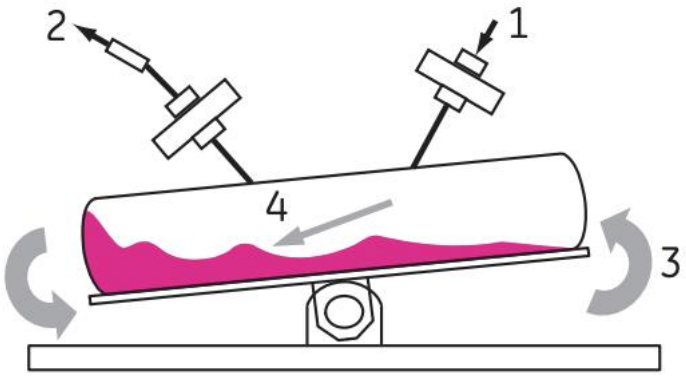

Figure 6.1.2.: Illustration of wave motion. (1) Inflowing gas; (2) Outlet metabolic waste gas; (3) Rocking mechanism; (4) Wave motion induced by rocking (GE Healthcare)

Reactor are shown below in Table 6.1.1 and were determined using the Wave 25 manual for *E. Coli* growth. Each day, six of the seed train apparatuses will complete their 35-hour fermentation cycle. Each of the six 150 L inoculated cell bags is then fed to one of the six bioreactors. This allows for a continuous 36-hour cycle alternating between seed train and bioreactors. Both the pneumatic wave rocker and bioreactor utilize single-use disposable reactor bags to allow for minimal cleaning. The use of cellbags also significantly cuts down the water and energy costs associated with cleaning the reactors. Each wave reactor scales the initial 1500 mL of high-density cell bank to an output of 150 L. An additional hour was added to the reaction time to account for maintenance, loading, and cleaning.

Table 6.1.1: Operational Conditions for GE Pneumatic Wave25 Rocking Bioreactor

Rocking Speed (RPM)	25
Rocking Angle (°)	10
Temperature (C°)	37
Batch-Process Time (h)	36
pH	7
% Oxygen in headspace	30
% Nitrogen in headspace	70
Power Required (kW)	12
Flow Rate for Aeration (L/h)	120
High Density Cell Culture Feed (mL)	1500
Growth Medium (L)	150
Ampicillin (g/L)	35

6.2. Bioreactor

In a semi-batch or fed-batch reactor, Monod kinetics utilize the exponential nature of bacterial growth to predict rates of production and consumption of substrate. The dynamic behavior of a fed-batch system is beyond the scope of this project and therefore, was simplified into a quasi-steady state (QSS) kinetic model, reflected in Equations 6.2.1 through 6.2.5. The simplifications associated with the QSS model include (1) assuming a linear feed rate, as opposed to a batch or variable feed rate, and (2) assuming the specific growth rate of *E. coli* is equal to the dilution rate, as expressed in Equation 6.2.5. These QSS assumptions were used to model Figure 6.2.1 for a 35-hour semi-batch reaction where the resultant growth rate increases linearly as a consequence of assumption 1. This linear growth rate can be used in Equation 6.2.3 to determine substrate mass over time and 6.2.4 to determine product mass over time.

The four differential equations which govern a semi-batch reactor using QSS assumptions are shown below in Equations 6.2.1-6.2.5. These equations were solved as an initial value problem in which the starting volume, feed rate, substrate, and cell mass dictated the dynamics of the process.

$$(6.2.1) \quad \frac{dX^t}{dt} = (\mu - \frac{F}{V})X^t$$

$$(6.2.2) \quad \frac{dV}{dt} = F$$

$$(6.2.3) \quad \frac{dS^t}{dt} = \frac{-1}{Y_{xs}}\mu X^t + S_o F$$

$$(6.2.4)\quad \frac{dP^t}{dt} = \frac{1}{Y_{xp}}\mu X^t$$

$$(6.2.5)\quad \mu = \frac{F}{V}$$

The relationship between growth rate of total cell mass, $\frac{dX^t}{dt}$, measured in g/h to the specific growth rate, μ, dilution rate $\frac{F}{V}$, and total cell mass X^t measured in g/h, is shown in Equation 6.2.1.

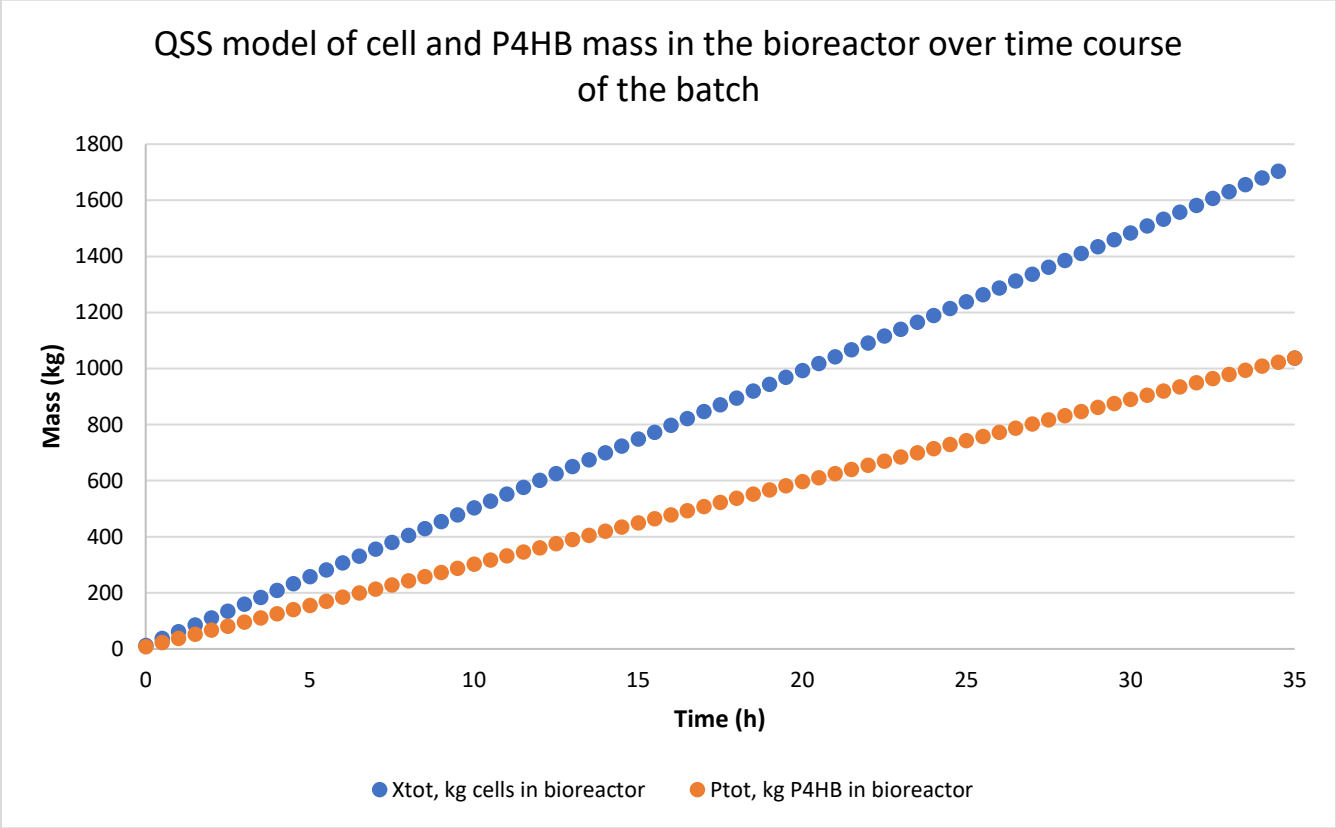

Figure 6.2.1: Quasi-Steady-State (QSS) model of cell and P4HB mass in bioreactor over a 35-hour reaction

The rate change of liquid volume within the reactor is determined by the reactor linear feed rate, F, measured in L/h, as shown in Equation 6.2.2. The use of a semi-batch fed bioreactor allows for a linear increase in the total mass of cells while the concentration remains relatively the same, which is balanced by dilution (D). For a QSS reaction, it is assumed that the rate of dilution is equal to the specific growth rate of *E. coli*.

Equation 6.2.3 is used to determine the rate of change in the total dissolved substrate, in grams, by subtracting the rate of substrate consumption from the rate of substrate fed. S^t demonstrates the total mass of the rate limiting substrate. Since the large quantity of cells will quickly consume the substrate as it is added, Equation 6.2.3 is essentially equal to zero. The substrate consumption is calculated by the first term where $Y_{xs}\frac{g\ CDW}{gSubstrate}$. The conversion factor between cell mass and substrate consumed, Y_{xs}, remains constant. The rate of substrate fed is calculated such that S_0 is the feed's substrate concentration measured in g/L. Equation 6.2.4 relates the rate of total product produced, P^t, measured in grams, to μ, X^t, and $Y\frac{gCDW}{gP4HB}$, where $Y_{xp}\frac{gCDW}{gP4HB}$ (Faghihzadeh, F. et al., 2018) was used to determine the production rate shown in Figure 6.2.1. Bacteria in the accumulation phase utilize substrate consumption to store energy in the form of P4HB granules with a consistent ratio of P4HB stored to cell mass between 60-70% (w/w). The published studies were all published as a single-batch process. Experimental data shows that reactions surpassing the 35-hour mark is when cell death starts to occur (Le Meur et al., 2013).

Governing equations, shown in Table 6.2.1, were used to create the reactor design and material balances for the upstream reactions were performed with the Monod reaction kinetics for *E. coli* at 37 °C. Optimal values for oxygen flow rate and impeller speed were found to satisfy all governing equations shown. The superficial velocity, υ_s, should be kept under 125 m/h to prevent gas slugging, which happens due to large, non-uniform pockets of gas that form as a result of excessive aeration. Gas slugging will hinder gas diffusion and has the potential to disrupt cells. The volumetric aeration rate, Q_g, is constrained by the inequality shown is to prevent gas flooding. Gas flooding would occur if the fed gas collects under the surface of the impeller, resulting in poor gas dispersion. Hold up (ϕ) relates the volume of gas in the reactor compared to the liquid volume. This relationship is essential

Table 6.2.1: Governing equations for bioreactors of standard geometry.

Variable:	Equation:	Rules to satisfy:
Superficial Velocity (υ_s)	$(v_s) = \frac{Q_g}{\pi {D_t}^2/4}$	υ_s < 125 m/h to prevent gas slugging
Volumetric Aeration Rate (Q_g)	$Q_g \leq 0.6(\frac{D_i^5 N^2}{{D_t}^{1.5}})$	Prevents gas flooding
Hold Up (ϕ)	$(f) = 1.8 P_m^{0.14} (n_s)^{0.75}$	Prevents excessive foaming due to aeration
Number of Impellers (n_i)	$\frac{H_l - D_i}{D_i} \geq n_i \geq \frac{H_l - 2D_i}{Di}$	$3 \geq n_i$
Tip Speed	Impeller tip speed $= \pi N D_i$	For proper gas dispersion > 2.5 m/s
Power Input for Gassed System per Tank Volume	$\frac{P_g}{V}$	$\frac{P_g}{V} < 15{,}000 \frac{W}{m^3}$

for ensuring there is sufficient headspace within the reactor. A headspace that is 10% of the gassed volume will be used to ensure that sufficient headspace is provided. The number of impellers and impeller tip speed were chosen to ensure consistent flow and that sufficient shear rate is provided to achieve a desired aeration rate. The power input for the gassed system is used to verify that the power consumption is reasonable for its intended scale. These values were found by using the Goal Seek function in Excel to ensure all values and rules of Table 6.2.1 were satisfied.

The overall batch process time of 36 hours was determined through previous studies, which includes cleaning cycles, 2544 batches can be run per year. The 15,000 L I-Series bioreactors, sourced from Solaris, include pH, temperature, and gas sensors. Each of the bioreactors will be monitored and controlled with an ethernet machine connecting parallel machines, allowing for a single computer to be used for process control and gas analyzing software. The temperature of the bioreactor will be maintained at a constant 37 °C via a cooling water jacket. A double jacket, equipped on both side and bottom of the vessel, heat exchangers, and recirculating. The pH of the broth will be maintained at 7.0 ± 0.1 by automatic additions of 25% NaOH or 30% H_3PO4. A 35-hour, continuous-fed, batch reaction will occur in each bioreactor. A minimum oxygen content of 30% saturation will be maintained through sparging rates determined by oxygen probes and process controls. Biomass growth can be monitored throughout the fermentation cycle with optic density probes.

The growth medium used to inoculate the preculture and grow the *E. coli* will contain the following additives: 3.5 g/L of $NaNH_4HPO_4 \bullet 4H_2O$, 3.7 g/L of KH_2PO_4, 7.5 g/L of

K_2HPO_4, and 10 g/L of cheese whey. As an undesired and abundant bi-product obtained by precipitation and removal of milk casein during the processes of making cheese or yogurt, whey makes an economical carbon source for the production of P4HB (C. Reddy et al., 2003). The boosted demand for Greek yogurt, starting around 2005, led to an extreme increase in the excess of whey, and in turn, raised many environmental concerns for its disposal, which makes it a desirable feedstock for bioproduction (Amaro et al., 2019). Waste whey contains most of the lactose of milk (around 46 g/L) and will require deproteination through ultrafiltration and requires sterilization before use (Viitanen et al., 2003).

$$(6.2.6) \quad Re = \frac{\rho_L N_{stir} D_i^2}{\mu_L}$$

The equation for calculating the Reynold's number (Re) is shown in Equation 6.2.6, where N_{stir} is the impeller speed rotation in s^{-1}, D_i is the impeller diameter in meters, viscosity (μ_L) is given in Pa•s. The fermentation process will be assumed to have a constant density (ρ_L) and viscosity (μ_L), which can be approximated using the properties of water. The power number (N_P) is used in fluid tanks to calculate power transfer, as shown below in Equation 6.2.7, where P_g is the power in a gassed system, given in W.

$$(6.2.7) \quad N_p = \frac{P_g}{\rho_L N^3 D_i^5}$$

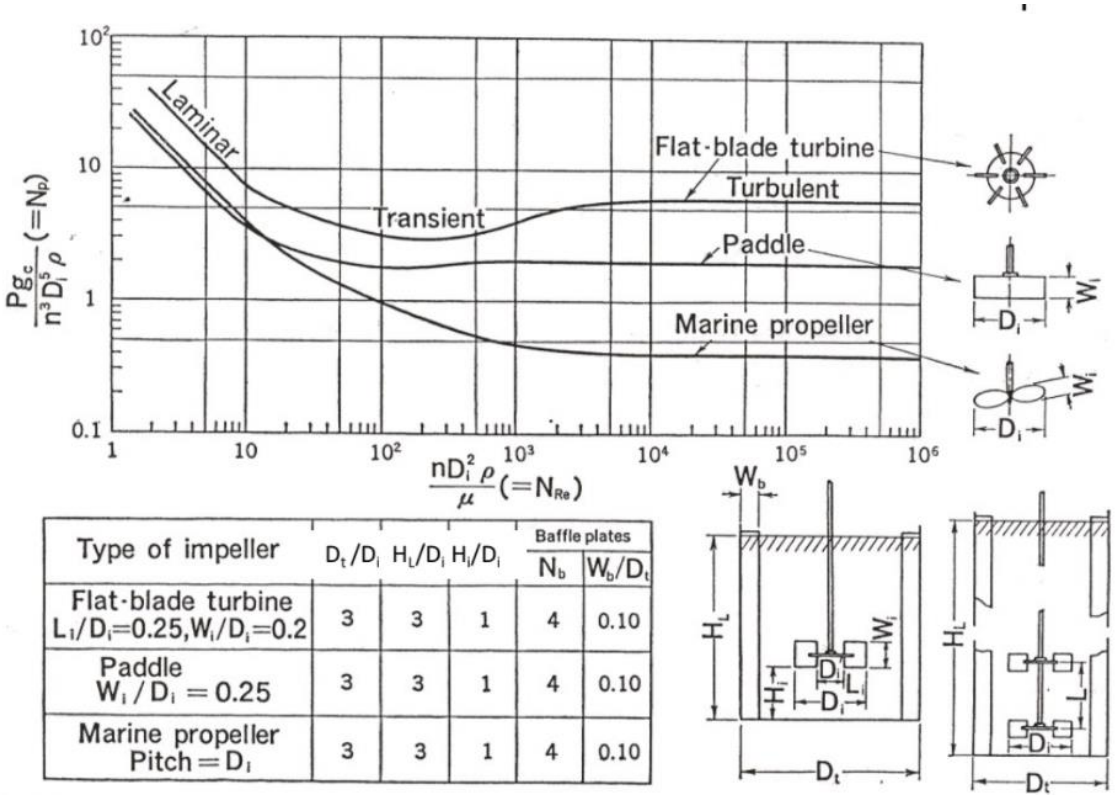

Type of impeller	D_t/D_i	H_L/D_i	H_i/D_i	Baffle plates N_b	Baffle plates W_b/D_t
Flat-blade turbine $L_i/D_i=0.25, W_i/D_i=0.2$	3	3	1	4	0.10
Paddle $W_i/D_i=0.25$	3	3	1	4	0.10
Marine propeller Pitch $=D_i$	3	3	1	4	0.10

Figure 6.2.3: Rushton Curves for a tank with standard geometry (Rushton, et al.)

Using the calculation of the Reynold's number, Ruston Curves were used to find N_p, with impeller geometry, as shown above in Figure 6.2.3. The physical properties of the tank were found using standard tank geometry, where the tank diameter (D_t) and tank height (H_t) are given in meters. The ratio of D_t to H_t will always equal one, and D_i is equal to 1/3 D_t. The bioreactor will be constructed with 316 stainless steel and a 25RA finish. Thermal mass flow controllers will be used to monitor precise flowrate of individual gasses. Upstream processes consume power for reactor mixing and temperature control. The mixing power is dependent on the reactor size and providing sufficient aeration. Impeller diameter, impeller speed, gas flow rate, and fluid properties determine the diffusion rate of oxygen throughout the fermentation media and directly impact the mixing power. Equation 6.2.7 is used to calculate the mixing power and then adjusted for change in volume due to

suspended gas. The corrected gassed volume power value is then multiplied by the number of impellers, giving the total power consumption of the bioreactor. The calculated mixing power, operation time, and batch schedule can then be used to estimate daily and yearly power consumptions for use in economic analysis. The fermentation process generates heat at a rate proportional to total cell mass and integration of the heat flow curve provided total fermentation heat flow. The compilation of specific properties of the bioreactor are listed below in Table 6.2.2. The growth kinetics for *E. coli* K12, adapted from (Le Meur et al., 2014), are shown below in Table 6.2.3. An additional hour was added to the reaction time to account for cleaning, loading, and maintenance.

Table 6.2.2: Bioreactor Specifics of I-Series 15,000 L Reactor from Solaris.	
Tank Area (m^2)	5.611
Turbine Type	Rushton Baffled Impellers
Number of Impellers	2
Tank Diameter | D_T (m)	2.67
Impeller Diameter | D_i (m)	0.891
Impeller Spacing | D_i (m)	0.891
Wall thickness (m)	0.222
Gassing Factor	0.49
Reynolds Number	Turbulent Range

Table 6.2.3. Reaction Kinetics and Monod Parameters for P4HB production in *E. coli*		
μ_{max}	Maximum Growth Rate (h^{-1})	0.76
K_s	(g/L)	3.28E-05
Flow Rate Feedstock	(L/h)	424.29
Initial Reactor Volume	(L)	150
Reaction Time	(h)	35
Starting Concentration	(g Cheese Whey/L)	215
Oxygen Saturation Concentration	(mg/L)	6.578
K_{la}	Oxygen Transfer Rate (s/m^3)	0.0157
N	Impeller Speed (s^{-1})	1.67
Q_g	Volumetric Flow Rate of Oxygen (m^3/h)	0.2
Yield data:		
Yield of P4HB to Cells	(w/w | mass basis)	0.6
Yield of Cells to Substrate	(w/w | mass basis)	0.5
Final Product Concentration	(g/L)	3

6.3 Mixing Tanks for Feedstocks

The first mixing tank will contain the feedstock mixture and will be the largest of the three tanks. The second stir tank will mix the solid activated charcoal particles with deionized water, which will be used as a feed for the third mixing tank. The two mixing tanks, MT-1 and MT-2 will be run 24 hours a day in order to maintain the feedstocks needed for daily processing. Table 6.3.1 shows the operating conditions for these two mixing tanks. The power for the mixing tanks was determined using Equation 6.3.1 where D_t is the diameter of the tank.

$$(6.3.1)\quad Power = (RPM)^3 D_t^5$$

Table 6.3.1. Feedstock Mixing Tank Operational Parameters	
Mixing Tank 1	
Capacity (L)	113,000
Top Head	Split
Head	Cone
RPM	50
Maximum Retention Time (h)	24
Turbine Type	Axial Flow Turbine
Turbine Diameter (m)	0.25
Power Requirement (kW)	1.2
Mixing Tank 2	
Capacity (L)	10,000
Top Head	Split
Bottom Head	Cone
RPM	50
Maximum Retention Time (h)	24
Turbine Type	Axial Flow Turbine
Turbine Diameter (m)	0.2
Power Requirement (kW)	0.4

7. DOWNSTREAM PROCESSES

The physical properties of the bioparticle containing the P4HB granules used to calculate downstream processing are shown below in Table 7.1. The density of the fluid was assumed to be equal to the density of water. The density of the E. Coli broth, $\rho_{cells,}$ at and OD of 60 was found to be 1,220 kg/m^3 and the viscosity of the cell solution, (η_L), was based on previous studies (Zhou et al., 2012). Sedimentation velocity (Vg) was found using Equation 7.1, using the values in Table 7.1.

$$(7.1) \quad V_g = \frac{4r_p^2(\rho_p - \rho_{fluid}) * g}{18\eta}$$

Table 7.1. Physical Properties of *E. coli* Post-Fermentation	
Radius (r_p) | mm	0.5
Density (ρ_p) | g/cm^3	1.2
Sedimentation Velocity (V_g) | cm/h	0.02
Reynold's Number of Particle	1E-13
η_L (cP)	4.5
ρ_{fluid} (kg/m^3)	1,000
ρ_{cells} (kg/m^3)	1,220
(Don W. Green & Robert H. Perry, 2008)	

7.1. Centrifugation

Following fermentation, the cultivation broth is fed to the rotating disc centrifuge. Sedimentation velocity is based on the radius (r_p) of an isolated sphere of *E. coli* and its density (ρ_p), suspended in a fluid with viscosity (μ_L) and a different density (ρ_L) than the sphere. The intracellular P4HB is harvested from the cells by fluid-solid separation, relying on the small difference in density between the cells, cultivation broth, and desired product. The sedimentation velocity for *E. coli* was found by integrating Equation 7.1.1, where g represents gravitational acceleration. The sedimentation coefficient, S, was found using Equations 7.1.1 – 7.1.6. The centrifugal force was found using Equation 7.1.6, where ω is in rad/s and r_p is the distance from center rotation.

$$(7.1.1)\quad m\frac{dv}{dt} = \sum F = F_G - F_B - F_D$$

$$(7.1.2)\quad F_G = \frac{4}{3}\pi r_p^3(\rho_p) * g$$

$$(7.1.3)\quad F_B = \frac{4}{3}\pi r_p^3(\rho_L) * g$$

$$(7.1.4)\quad F_D = 6r_p\eta v$$

$$(7.1.5)\quad S = \frac{v_g}{g} = \frac{4(\pi r_p^3)(\rho_p - \rho_f)}{18\mu_L}$$

$$(7.1.6)\quad F_\omega = \frac{4}{3}\pi r_p^3 \rho_p \omega^2 r$$

A stacked disk centrifuge will be used to accommodate a large capacity of solids, discharging the solid stream, which will contain mostly P4HB, but will require further purification. The centrifuge can be cleaned in place between runs with a caustic solution run. Operating conditions for the rotating disk centrifuge are shown below in Table 7.1.1.

The design of the centrifuge is show in Figure 7.1.1 and will process six bioreactor volumes, totaling to 90,000 L of cell broth per day.

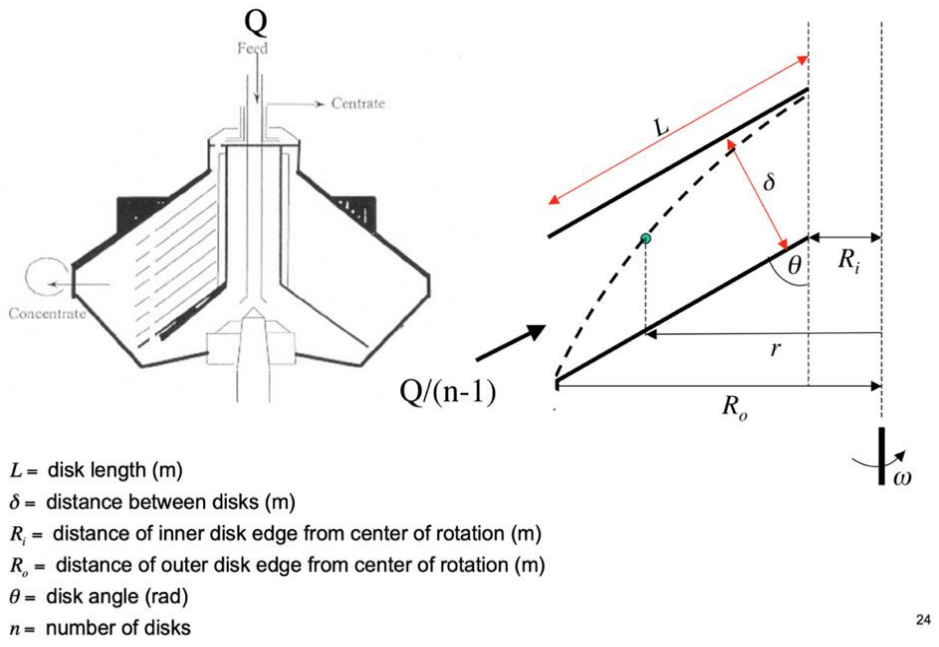

Figure 7.1.1: Disk Stack Centrifuge Diagram (Carta)

Table 7.1.1. Disk Stack Centrifuge Operating Conditions	
Bowl Diameter (m)	0.61
RPM	3000
Centrifugal Force (rad/s)	540
Power (kW)	5.59
Max Through-put (L/h)	45,424
# discs	50
Disc Angle (°)	45
Disc Length (m)	1
R_i (m)	0.1
R_o (m)	0.3
d (m)	0.2
(Don W. Green & Robert H. Perry, 2008, 21-8)	

7.2. Homogenization

Following centrifugation, the cultivated cell broth containing the P4HB with remaining cell debris is fed through the homogenizer. To ensure cells are properly lysed and a homogenous slurry is made, *E.coli* bacteria requires a pressure of 1034 bar (Don W. Green & Robert H. Perry, 2008). The physical shear stress applied to the cells ruptures any cells that have remained intact following centrifugation. The high operational pressure of the homogenizer requires an extensive amount of energy, which will increase operational costs, however, it ensures a single pass through the system will provide sufficient homogenization. Liquid fed to the homogenizer flows between the valve and seat at a high velocity, which produces an instantaneous pressure drop. Then, the liquid impacts on the wear ring before being discharged as a final product. A positive-displacement pump and the actuating force of the valve forced against the seat generate the pressure in the system,

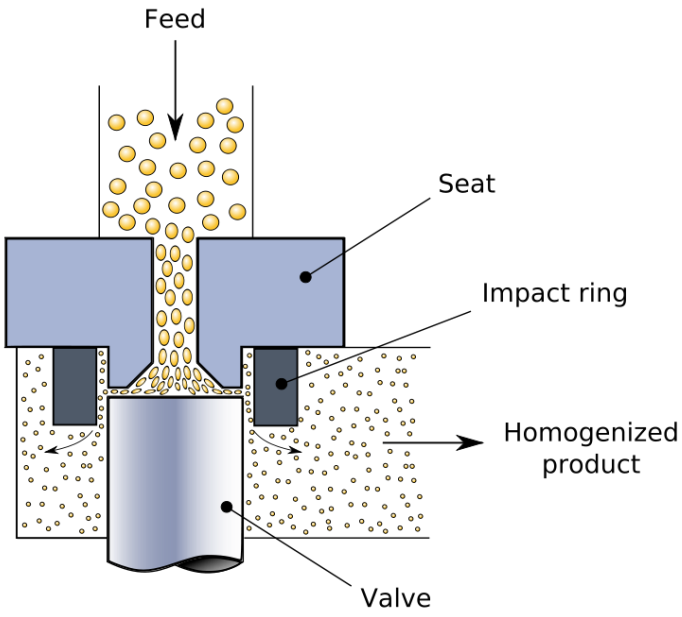

Figure 7.2.1: Homogenization mechanics. ScienceDirect.com

as shown in Figure 7.2.1. The angle of the seat allows for the liquid to accelerate in a

controlled way. The piston pump generates a pulsating flow, and the acceleration and deceleration of the mixture creates pulsating pressure in the suction pipe. A jacketed homogenizer allows for cooling water to keep the slurry around 32 °C because for every 40 bar of pressure drop within the homogenizer will rise the temperature of the fluid by 1 °C.

$$(7.2.1) \quad V_g = \left(\frac{r_P^2 \left(\rho_{fluid} - \rho_P \right)}{18 * \mu_L} \right) * g$$

The efficiency of the homogenization with Stokes' Law, as shown in Equation 7.2.1, using the values from Table 7.1. The flow rate for the homogenizer can be simplified to in equals out. The operational conditions for the homogenizer are shown in Table 7.2.1.

Table 7.2.1. Homogenizer Operating Conditions	
Pressure (Bar)	1034
Maximum Flow Rate (L/h)	10,000
Number of Plungers	5
Stroke (nm)	150
Power (kW)	315
Heat Transfer Rate (kJ)	6,281
Cooling Water (L/h)	430
Source: GEA Ariete Homogenizer	
https://www.gea.com/en/products/homogenizers/industrial-	

7.3. Mixing

The downstream mixing tank, MT-3, will be used to mix the 9,706 L of homogenized P4HB slurry with 75% of its volume, in liquid activated charcoal. The liquid activated charcoal binds to impurities in the mixture so that pure P4HB can be removed during

filtration. The mixture will stir for one hour, before being fed to the filtration unit. Mixing tank parameters are shown below in Table 7.3.1.

Table 7.3.1. Mixing Tank Operational Parameters	
Mixing Tank 3	
Capacity (L)	20,000
Top Head	Cone
Bottom Head	Slope
RPM	100
Maximum Retention Time (h)	1
Flow Pattern	Radial Flow Impeller
Turbine Diameter (m)	0.2
Power Requirement (kW)	3.2

The power requirement for each tank was found using Equation 7.3.1, where the impeller diameter is given in meters.

$$(7.3.1)\quad Power = (RPM)^3 D_t^5$$

Axial flow turbines were chosen for stir tanks one and two to ensure proper solid-liquid mixing of raw materials and deionized water. Each blade will be pitched at a 45-degree angle, creating a localized shear to maximize mixing. Mixing tank three will have radial flow impellers, ensuring flow collides along the sides of the tank, then moving in an upward flow to mix fluid. Mixing tank one and two have cone shaped bottom heads to allow for easy drainage from the solid-liquid mixing tanks and split top heads to allow for both a solid and liquid feed. Mixing tank three will have a sloped bottom head, allowing for easy draining of the slurry, and will have a cone top head to allow room for radial flow throughout the vessel. Each tank will be made with 316 stainless steel and be polished with a 25RA – finish certification.

7.4. Filtration

E. coli has no membrane organelles, thus, the P4HB is released when the cells rupture with other large extracellular cell debris. The large cell debris and particle size of the activated charcoal make filtration simple. The solubility of P4HB within a liquid activated

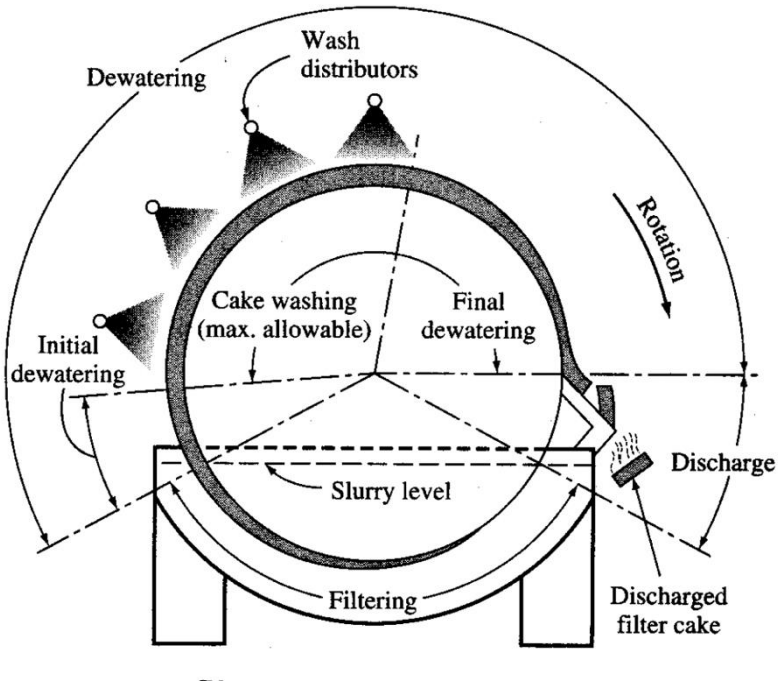

Figure 7.4.1: Rotary Filtration Diagram (Carta)

charcoal slurry enhances the ability of phase separation techniques with porous devices. Phase separation will be accomplished through use of pressure filtration and a filter medium made from metallic lace tissue. Filtrate will be passed through a 0.45 μm membrane filter to remove any remaining impurities, such as fine charcoal particles, cell debris, and other particulate matter. The filtration unit is used to separate cellular debris, impurities, and the liquid activated charcoal through phase separation. The phases were

separated by pressure filtration through a metallic lace tissue (Wampfler et al., 2010). Design schematics are shown above in Figure 7.4.1.

Filtration requires a three-hour operation time for one day of production . The built-in cake washing system along with metallic lace filters ensure that pure P4HB is separated out from any remaining impurities, such as, cell membranes, intracellular proteins, charcoal particles, and genetic material. The fundamental equation to describe the flow through the filtration is given by Darcy's Law, as shown below in Equation 7.4.1, where ν is the fluid velocity in m/s, ΔP is the applied pressure in Pa, is the liquid viscosity η in Pa*s, and R is the flow resistance parameter in m^{-1}. Figure 7.4.2 depicts the relationship between Darcy's Law and the filtration system. The resistance flow parameter, R, is the sum of two

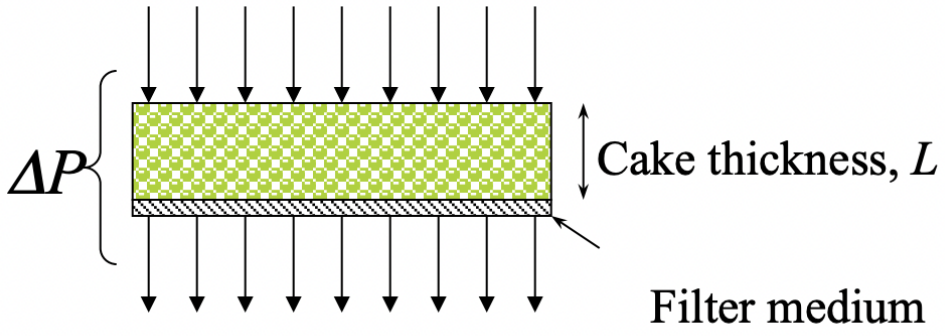

Figure 7.4.2: Calculating pressure drop between cake thickness and pressure for use of Darcy's Equation

terms; R_m, which remains constant, is the filter medium resistance, and R_c, which will vary over time, is the filter cake resistance. The cake resistance parameter is shown below in Equation 7.4.2, where α is the cake resistance parameter in m^{-2} and L is the cake thickness in m. The cake parameter resistance will vary with the shape of the particle and is dependent upon how densely packed the cake is, and higher α are found for small particles and dense cakes. The filtration system operates under hermetic conditions to ensure no

product is wasted and eliminates the risk of contamination. The design equations relevant to the filtration unit are shown below in Equations 7.4.1 – 7.4.6. Figure 7.4.3 shows the relationship to each parameter to the filtration system. For these equations, V_b is given in m^3, and represents the suspension volume within the filtration system, the slurry

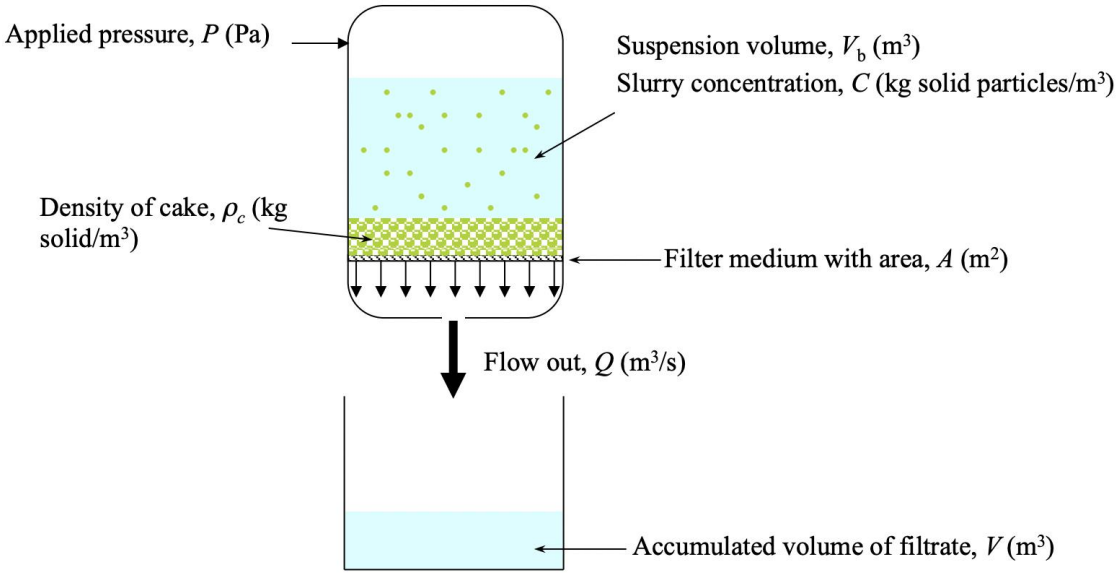

Figure 7.4.3: Design and variable relationships for filtration calculations. (Carta)

concentration, C, is given in kg solid particles/m^3, ρ_c, given in kg solid/m^3, represents the density of the cake, A, given in m^2, is the area of the filter medium, Q, given in m^3/s, is the flow out of the filtration system, and *V*, given in m^3 is the accumulated volume of the filtrate. The filtration system is designed with a tight thermal insulation and welded with a stainless-steel cover. Also contained within the system are condensation systems, vacuum, and heating units. Equation 7.4.6 shows the overall material balance on the filtration system.

$$(7.4.1) \quad v = \frac{1}{R}\frac{\Delta P}{\eta}$$

$$(7.4.2) \quad R_c = \alpha L$$

$$(7.4.3)\ R_c = \alpha L = \alpha \frac{CV}{\rho_c A}$$

$$(7.4.4)\ R = R_m + \alpha \frac{CV}{\rho_c A}$$

$$(7.4.5)\ Q = v\alpha = \frac{A\Delta P}{\eta R}$$

$$(7.4.6)\ C * Q * t = CV = \rho_c LA$$

Using these design equations, the operating conditions for the filtration unit were determined and are shown below in Table 7.4.1. Each day the filtration system will need to run for three and a half hours, during which the slurry of P4HB and activated charcoal fed to the system is separated into waste as well as the P4HB product to be dried. The waste stream leaving the filtration unit accumulates around 9,800 L of waste per day. In the fully automatic three-hour filtration cycle, the P4HB biomass is first filtered, then re-dissolution with deionized water and washed to obtain a high purity and homogenous final product.

Table 7.4.1. Filtration Unit Operating Conditions	
Filter Surface Area (m^2)	15
Operational Capacity (L)	15,000
Operational Type	Continuous
Time (h)	3
Pressure (Bar)	3
Temperature (°C)	37
Bottom Filter Waste Flowrate (L/h)	3,270
Power Requirement (kW)	325
Source: https://bachiller.com/en/nutsche-filter/#features	

7.5. Drying

During filtration, the PHAs are isolated by direct concentration of the filtrate without prior precipitation (Wampfler et al., 2010). The resulting polymer mass is quenched before extrusion, with stretch ratios six to 11 times over a multistage drying process. This drying process forms the suture fiber and creates the desired tensile strength and handling properties for medical use. First, the polymer mass will be fed to a rotary drier for a twelve-hour batch process in which 95% of the moisture is removed. Direct rotary dryers are the most common equipment choice for drying bulk solids as the direct contact between the material and drying air maximize the heat transfer and increasing the efficiency of the process. The minimum heat supply rate (Q_y) for each dryer was found using Equation 7.5.1 where the heat of formation for P4HB is 76 J/kg. The required energy per batch, in Joules, is then found with Equation 7.5.2, where the heat capacity of P4HB is 159 J/mol*K, where the molecular weight of the repeating unit is 86.1 g/mol (Polymerdatabase.com).

$$(7.5.1)\quad Q_y = (kg\ P4HB\ in - kg\ P4HB\ out) * \Delta H_v$$

$$(7.5.2)\quad Q_{in} = \left(kg\ P4HB\ in * \ Cp_{P4HB} * (T_2 - T_1)\right) + Q_y$$

Following the rotary dryer, the remaining 5% of moisture is removed from the P4HB in a sanitary vacuum dryer for a 24-hour batch process. The secondary vacuum dryer protects the desired properties of the P4HB Both dryers will be made with 316 stainless steel with a 25RA finish, have floating mechanical seals flushed with nitrogen, and meet FDA guidelines for sanitary design. The operating conditions for the dryers are show below in Tables 7.5.1 and 7.5.2.

Table 7.5.1. Rotary Dryer Operating Conditions	
Diameter (m)	1.2
Length (m)	7.5
Capacity (Metric Tons)	18
Q_y (J)	5594
Power Requirement (kW)	10
Moisture Removal	10%
Temperature (C)	45
Pressure (mBar)	200
Time (h)	12
Source: https://feeco.com/rotary- s/	

Table 7.5.2. Sanitary Vacuum Dryer Operating Conditions	
Horizontal Paddle Vacuum	
Operation	Batch
Capacity (Metric Tons)	10
Vacuum Pressure (mBar)	1
Operating Pressure (atm)	1
Moisture Removal	5%
Temperature (C)	40
Q_y (J)	2409
Power Required per Batch (kW)	15
Time (h)	24
Source: https://bachiller.com/en/sanitary-vacuum-paddle-dryer-sanidry/#applications	

7.6. Extrusion

Blown film extrusion was chosen due to the ability to handle the heat sensitivity of P4HB while shaping the dried polymer mass into rolls of the thin film optimum for distribution. Blown film extrusion is almost exclusively done one single screw extruders where the extrudate flows through an annular die, forming a bubble or tube that is pulled away from the die vertically as the polymer is air cooled (Giles et al, 2005). Upon exiting the die, the polymer forms a bubble which can be blown to different diameters, allowing different films widths to be produced with the same die. An air ring at the die exit and possibly internal bubble cooling can be used to solidify the polymer melt. The stability of the complex process is affected by many variables, such as, the rate of bubble cooling, the stability of the bubble, the frost line height, the temperature and flow of air, the bubble sizing cage and collapsing frame, tension control, and type of winder. The cooling rate is determined by air flow, film speed, and the temperature difference (Giles et al, 2005). The frost line height is the point at which the film changes from the melt to a semicrystalline polymer, and can be seen visually, as the film changed from a transparent amorphous state to a translucent crystalline structure (Wagner et al., 2014b). To produce the film the P4HB is fed to the extruder through a hopper, where heat and friction are used to melt the polymer. The melted polymer is then forced through a ring-shaped die to form a tube. The tube, which is also called a 'bubble', is then inflated to decrease the film gauge and increase the diameter. Simultaneously, the tube is also drawn away from the die, stretching the bubble axially and radially. The bubble is then flattened while being forced through a collapsing frame and then drawn through the nip rolls. Finally, the polymer can be run over idler rolls and onto a winder to produce the final product. An overview of this process is

shown below in Figure 7.6.1. The finished rolls of P4HB film will be ready to be shipped for sterilization.

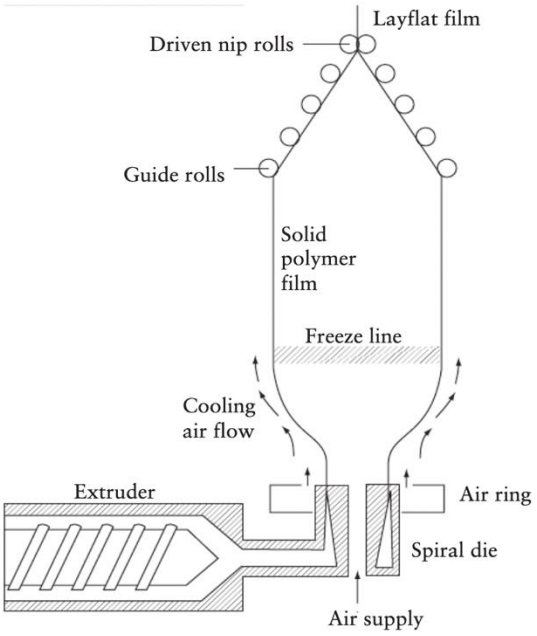

Figure 7.6.1: Blow film extruder process from Vlachopoulos et al. 2012

To ensure a high-quality extruded film, the parameters of melt orientation theory were used. Three ratios govern melt orientation theory, the blow-up ratio (BUR), the drawdown ratio (DDR), and the blow ratio (BR) (Vlachopoulos et al., 2012). BUR, shown in Equation 7.6.1 is the ratio of bubble diameter to die diameter and is indicative of the expansion of bubble diameter in the transverse direction, -that is, over the die diameter- and should be between two and five to ensure proper extrusion.

$$(7.6.1)\ \ BUR = \frac{Final\ Bubble\ Diameter}{Die\ diameter} = \frac{D_B}{D_D} = \frac{2 * Lay\ Flat\ Width}{\pi * D_D}$$

Lay flat width (LFW) is the collapsed bubble width before slitting and is given by Equation 7.6.2 below.

$$(7.6.2)\ \ LFW = \frac{\pi * D_D * BUR}{2} = \frac{\pi * D_B}{2} = 1.57 D_B$$

DDR, shown in Equation 7.6.3, is the drawing taking place in the film tower in the machine direction and compares the final thickness reduction in the melt after blowing. Higher draw ratios are indicative of relatively higher final film velocity.

$$(7.6.3)\ \ DDR = \frac{Width\ of\ Die\ Gap}{Film\ Thickness} * BUR$$

The blow ratio is the increase of LFW over the die diameter. The power consumption of the extruder is dependent on the mechanical power needed to drive the polymer and the power needed to melt the polymer to the desired temperature (Giles et al, 2005). The blow ratio is the increase of LFW over the die diameter. The power consumption of the extruder is dependent on the mechanical power needed to drive the polymer and the power needed to melt the polymer to the desired temperature. Power consumption of the extruder is defined as the polymer heat of fusion subtracted from the energy required to heat from the feed temperature to the melt temperature, shown in Equation 7.6.4 below and defined in Equation 7.6.5.

$$(7.6.4)\ \ Power = (\Delta H\ needed\ from\ feed\ to\ melting\ temperature) - (\Delta H_{fusion})$$

$$(7.6.5)\ \ Power = m * C_p * \Delta T(+(m * \Delta H_{fusion}))$$

The film was produced using a 63.5 mm spiral mandrel die. The film blow-up ratio was found to be roughly 2.7 and the final thickness was about 50 microns. Our P4HB formulation was converted into blown film using a 0.11 m Davis Standard extruder equipped with a mandrel spiral die operating with a screw speed of 1000rpm to produce a throughput of 2300 kg/h.

Polymer melt temperature is critical in the control of the extrusion process and optimizing the throughput while minimizing resin degradation. The four zones (TZ1-TZ4)

of the extruder were set at: 21/49/69/80 (°C) with a feed temperature of 20°C and a blowing zone temperature of 80°C. TZ-1 is water cooled to provide uniform resin flow, preventing premature melting or polymer sticking to the feed hopper or the feed throat opening. It also prevents premature melting in TZ-1, where a lubricating melt film might lead to feed problems later in the run. TZ-2 is normally set at 11–17 °C below the melting point of semicrystalline polymers, or 70 °C above the T_g of amorphous polymers. In TZ-2, the polymer is compressed and preheated as it moves forward to TZ-3. Temperatures are raised progressively in TZ-3 and TZ-4 to the desired polymer blown film temperature. The extruder operating conditions are shown below in Table 7.6. (Wagner et al., 2014a)

Table 7.6. Extruder Operating Conditions	
Size (m)	0.11
Drive Power (hp)	10
Throughput (kg/h)	2300
Production Time (h)	7
Power Consumption (kW)	293
Die Zone (C)	160
Die Gap (mm)	1
Final Film Thickness (μm)	50
Finish Roll Diameter (m)	1.5
Lay Flat Width (m)	0.27
Specific Die Output Rate (kg/h*mm)	48.9
Source: Davis Standards https://davis-standard.com/converting_system/blown-film/	

7.7. Sterilization

Sterilization of the polymer material is essential for use in medical applications. The use of a third-party sterilization company will be used to execute the sterilization process, which includes being exposed to a cold ethylene oxide sterilization cycle for two and a half hours as required by CDC guidelines, within ethylene oxide sterilization bags. The sterilization cycle starts with pre-conditioning, sterilization, and is completed with aeration, and has a sterility assurance (SAL) of 10^{-6}. The required SAL ensures that the terminal sterilization in medical devices specifies that the probability of finding a non-sterile unit is one in a million. Random samples are then tested via direct transfer to test media, using the USP standard test method <25>, which confirms sterilization (Centers for Disease Control and Prevention, 2019). Following aeration, the rolls of film will be vacuum sealed and stored in -20 °C cold storage until shipped to purchasers.

8. ANCILLARY EQUIPEMENT DESIGN

8.1. Pumps

Centrifugal pumps are needed to transport fluid mixtures into the bioreactor, mixing tanks, and between other process equipment such as the centrifuge and homogenizer. Centrifugal pumps, as depicted in Figure 8.1, were used for P-100 to P-108 due to their

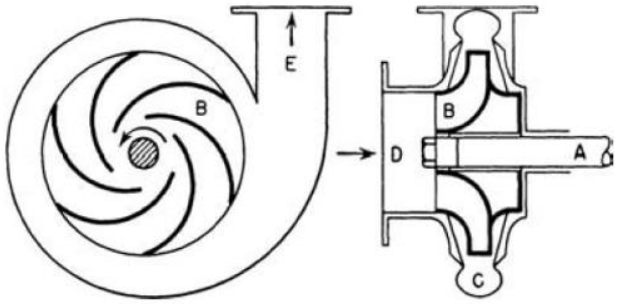

Figure 8.1.: A Simple Centrifugal Pump Design adopted from Perry's 8th edition

reliability and wide ranging of operations. A screw pump was used for transporting solids and slurries after the filtration unit. The screw pumps are pumps P-109 to P-111. The hydraulic power for each pump is dependent upon the energy needed to pump. The operating costs and capital costs for pumping equipment depend hydraulic power which is a function of the flow. The hydraulic power, P_H is the product of the flow rate of the fluid, Q_P pump which is often set by the material balances and batch schedule and the total differential of the pump, dP.

$$(8.1)\ P_H = Q_P \times dP$$

The total pressure difference is the sum of actual pressure difference between inlet and outlet (ΔP), losses due to friction (f_L), and the gravity head (H_g). The process is open to atmosphere meaning there is no difference in pressure between a source and destination for all pumps except for the filtration unit (FU-1). The pressure drop for the filtration is 300

kPa. The homogenizer operates above atmospheric pressure, but the equipment includes its own positive-displacement pump, and the resulting power is accounted within the unit. The frictional losses accounts for sum of losses through the piping and control valve, which were each estimated to be 0.5 atm (Anderson). Losses due to heat exchangers were accounted for through frictional losses as heat exchange occurs in line with the piping associated with the cooling or heating jackets for the unit operation equipment. The hydrostatic head (H_g) is the elevation difference of the pumped fluid when transferring material large tanks including the bioreactor and the three mixing tanks. The hydrostatic head was calculated using the height of each vessel (H_T) as shown in Equation 8.2 using the previously defined values of ρ_{fl} and g in section 7.1.1.

$$(8.2)\ H_g = \rho_{fl} \cdot g \cdot H_T$$

MT-1 is responsible for mixing the feedstock of all bioreactors and wave reactors. The height of the MT-2, MT-3, BR-1, are 2.34, 2.94, and 2.67 m tall, respectively. Table 8.1 shows the relationship between the pressure drop of each pump and location with respect to process equipment.

Table 8.1. Total Differential Pressure for Pumps						
Pump ID	*Inlet*	*Outlet*	*ΔP across equipment (kPa)*	*Frictional Losses, f_L (kPa)*	*Hydrostatic Head, H_g (kPa)*	*Total Differential Pressure Drop, dP (kPa)*
P-100		MT-1	0	101	51	152
P-101	MT-1	BR-1	0	101	27	127
P-102	WR-1	BR-1	0	101	27	127
P103	BR-1	CTF-1	0	101	0	101
P-104	CTF-1	HM-1	0	101	0	101
P-105		MT-2	0	101	23	124
P-106	HM-1	MT-3	0	101	29	130
P-107	MT-2	MT-3	0	101	29	130
P-108	MT-3	FU-1	300	101	0	401
P-109	FU-1	RD-1	0	101	0	101
P-110	RD-1	RD-2	0	101	0	101
P-111	RD-2	EXT-1	0	101	0	101

The efficiency of the pump, electrical driver, and the hydraulic power of the fluid dictates the electrical power requirement needed to operate the pump. The pump efficiency is assumed to be 70% and the electrical driver is 90% efficient (Anderson). Spares are included in capital costs, but not in operational costs as the spare pumps would only be used as a replacement for a non-functioning pump. The hydraulic power of the fluid is calculated using Equation 8.2 and is shown in Table 8.2.

Table 8.2. Power Requirement for Pumps			
Pump ID	**Flow Rate (L/h)**	**ΔP (kPa)**	**Power Requirement (W)**
P-100	37,666	152	2530
P-101	424	127	24
P-102	600	127	34
P-103	45,424	101	2030
P-104	9,706	101	434
P-105	10,000	124	548
P-106	10,000	130	573
P-107	20,000	130	1150
P-108	9,805	401	174
P-109	50,000	101	2230
P-110	50,000	101	2230
P-111	50,000	101	2230

9. ECONOMICS

9.1. Major Equipment Costs

Major equipment costs were calculated with data from (Petrides et al., 2014) with use of Equation 6a from (Turton, R. et al., 2009). Equation 9.1, shown below, was used to calculate the purchase cost of equipment, C_p, where A is an empirical the capacity parameter of the equipment and $K_{1\text{-}3}$ are constants found in correlations. The total major equipment costs are summarized below in Table 9.1.

$$(9.1) \quad log_{10}C_p^0 = K_1 + K_2 log_{10}(A) + K_3[log_{10}(A)]^2$$

Table 9.1. Total Major Equipment Purchase Costs

Tag	*Unit Name*	*Quantity needed*	*Cost per unit*	*Total Cost*
MT-1	Mixing Tank (113,000 L)	1	$257,000	$257,000
MT-2	Mixing Tank (10,000 L)	1	$25,000	$25,000
MT-3	Mixing Tank (20,000 L)	1	$50,000	$50,000
WR-1	Wave Reactor (150 L)	12	$548,000	$3,288,000
BR-1	Bioreactor (15,000 L)	12	$1,948,000	$11,688,000
CTF-1	Rotating Disc Centrifuge	1	$675,000	$675,000
HM-1	Homogenizer	1	$205,000	$205,000
FU-1	Filtration Unit	1	$136,000	$136,000
FUM-1	Filtration Membrane	1	$42,000	$42,000
RD-1	Rotary Dryer	1	$280,000	$280,000
RD-2	Vacuum Dryer	2	$425,000	$850,000
EXT-1	Extruder	1	$675,000	$675,000
Total Major Equipment Purchase Cost				**$18,171,000**

9.2. Total Plant Capital Costs

Total plant operating costs (TPC) are summarized below in Table 9.2. Direct costs are based on the given multipliers of the total major equipment purchase cost as described by Peters and Timmerhaus (Peters et al., 2003). Indirect costs are based on the given multipliers of the total plant direct costs. The TPC is then calculated as a sum of the total direct and indirect costs. Contractor and contingency fees are calculated from the given multipliers of TPC. The direct fixed capital (DFC) is a sum of the TPC and contractor and contingency fees.

Table 9.2. Total Plant Capital Costs

Direct Costs		% Capital Investment Cost
Equipment Purchase Cost	$18,171,000	35.4
Equipment Installation	$3,584,100	8
Instrumentation and Meters	$2,389,400	5.5
Piping and Installation	$1,593,000	3.5
Buildings & Land	$4,645,900	10
Electrical	$2,389,400	5.5
Yard Improvement	$796,400	2
Total Plant Direct Costs (TPDC)		$33,569,200
Indirect Costs		
Construction	$4,645,900	10
Engineering	$4,247,800	9.3
Total Plant Indirect Costs (TPIC)		$8,893,700
Total Plant Costs (TPC)		$42,462,900
Fees		
Contractor Fee	$1,592,900	3.6
Contingency	$3,185,800	7.2
Direct Fixed Capital (DFC)		**$47,241,600**

9.3. Operational Costs

The annual operational costs are summarized below in Table 9.3. Operational costs other than raw materials, sterilization, and electricity were calculated using Table 9.3 in Turton et al. and detailed explanations of the remaining operational costs are included later in this section. Solid waste disposal costs were approximated based on the dry weight of all used cellbags, disposable gloves, and single-use storage vessels. Raw materials including compressed oxygen will be purchased from vendors and the site will be equipped to supply deionized water . Wastewater treatment and disposal is needed for waste streams leaving the centrifuge and filtration units. Raw material costs are further expanded in section 9.3.3.

Table 9.3. Annual Operational Costs

Operating Costs	*Yearly Cost ($)*
Raw Material Supplies	$2,034,946
Sterilization	$16,956
Electricity	$671,530
Labor	$3,228,000
Deionized Water	$52,650
Oxygen Supply	$30,326
Wastewater Treatment and Disposal	$3,862
Waste Disposal	$100
Total Operational Costs Per Year	**$5,934,476**

9.3.1. Electricity

The estimated cost of electricity per year, is shown below in Table 9.3.1. Each major piece of equipment is represented by a Unit Tag. Costs also account for the use of 12 bioreactors, 12 wave reactors, and two rotary dryers. The price of electricity is assumed to be $14.50/GJ taken from the Average Price of Electricity to Ultimate Customers published by the US Energy Information Administration(*Electric Power Monthly - U.S. Energy Information Administration (EIA)*, n.d.).

Table 9.3.1. Estimated Costs of Electricity

Unit Tag	*Time (h)*	*Annual cost ($)*
WR-1 (12 units)	36	$1,957
BR-2 (12 units)	36	$108,775
CTF-1	2	$251
HM-1	1	$7,087
MT-3	1	$15,266
FU-1	3	$3,025
RD-1	12	$11,637
RD-2 (2 units)	24	$148,494
EXT-1	4	$8,000
MT-2	24	$636
MT-1	24	$366,397
Total Annual Electricity Cost		**$671,530**

9.3.2. Sterilization Costs

The estimated cost of third-party sterilization is $0.71 per 100 kg and was found using the upper bounds of ranges given in (Hagstrum, 2016). The yearly estimated cost for of third-party sterilization of 2,600 tons of polymer film is $17,000.

9.3.3. Raw Materials Costs

While the carbon-based feedstock normally accounts for a large portion of the operational costs, the unit cost of cheese whey is listed at zero dollars. Cheese whey, an abundant waste by-product of the dairy industry, is considered as a pollutant due to its high biological oxygen demand and its disposal is being managed at a considerable cost (Misra et al., 2018). By supplying whey as a carbon source, it eliminates the need for expensive, environmental treatment of dairy producer's waste streams. Fermentation of whey by microorganisms is one possible way of reducing the pollutant effect (Ricardo et al., 2000). For the purposes of this report, it can be assumed the whey will be supplied in the form needed for fermentation. The remainder of raw material prices were found through Quartzy and varying vendors. The cost of raw materials is based on the anticipated need of kilograms of material per year, as shown below in Table 9.3.3.

Table 9.3.3. Material Costs

Material	*Unit Cost (per kg)*	*Annual Amount (kg)*	*Yearly Cost ($/year)*
Glycerol	$0.15	779,976	$116,996
Whey	$0.00	3,075,000	$0
NaNH4 4H2O	$0.15	110,454	$16,568
K2HPO4	$0.49	116,883	$57,273
KH2PO4	$2.50	236,925	$592,313
Ampicillin	$3.00	1,556	$4,700
NaOH (0.5 M)	$0.14	940,000	$131,600
H3PO4 (5% w/w)	$0.25	850,000	$212,500
Activated Charcoal	$1.50	138,651	$207,977
150 L Cellbag	$30	2,106	$63,180
15000 L Cellbag	$300	2,106	$631,180
Total Yearly Cost of Raw Material Supplies			**$2,035,000**

9.3.4. Labor Costs

The operational cost of labor was calculated using Equation 9.3.4, where the number to processing steps that require handling of particulate solids is shown as P, the number of steps that do not require particulate processing are shown as N_{np} and N_{OL} are the number of operators per shift. Table 9.3.4 summarizes the annual labor costs of the three employee positions. Average annual salaries were estimated through LinkedIn and Glassdoor.

$$(9.3.4) \quad N_{OL} = (6.29 + 31.7P^2 + 0.23N_{np})^{0.5}$$

Table 9.3.4. Annual Labor Costs

Position	Number of Employees	Average Annual Salary	Yearly Cost
Operators	51	$50,000	$2,550,000
On-site Engineers	3	$76,000	$228,000
Managers	4	$150,000	$450,000
Annual Cost of Labor			**$3,228,000**

9.4. Anticipated Revenue

The anticipated revenue, as shown in Table 9.4.1, operates under the assumption that every kilogram of P4HB the factory produced is purchased at the current market value. This model also assumes that operating conditions to produce 7.65 tons of P4HB a day are met for 351 days per year. Current market information was adapted from (Misra et al., 2018) and adjusted for inflation to 2021. The gross revenue calculations account for the revenue in sales of P4HB in regard to the operational costs.

Table 9.4. Expected Revenue at Current Market Prices for P4HB ($/kg)	
Yearly Production of P4HB (tons)	2,685
Selling Price P4HB ($/kg)	$6.85
Total Revenue ($/year)	$18,390,270
Operational Costs ($/year)	$5,934,476
Operating Profit	**$12,381,015**

9.5. Return on Investment Analysis

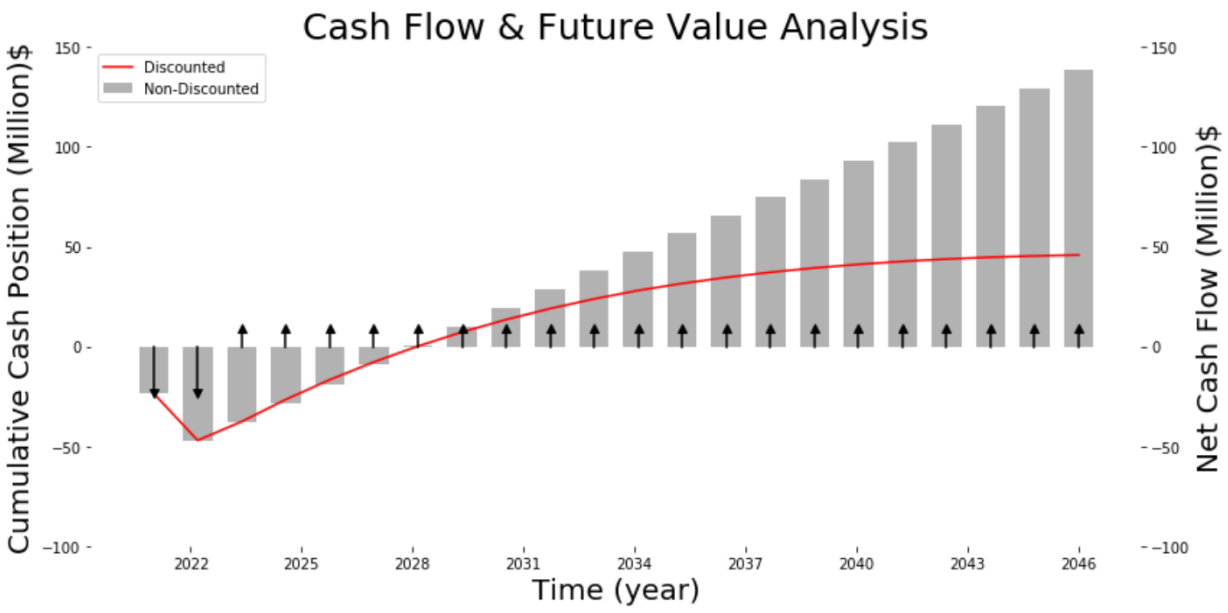

Figure 9.5: Cash Flow Analysis

Calculations for capital investments were estimated via methods described in Turton et al. for a 20-year plant life using a discount rate of 6% for projected future value. Figure 9.5 displays the resultant net cash flows, cumulative cash position, and discounted project value throughout the span of the plant timeline indicated by the black arrows, grey bars, and red line respectively. Depreciation was calculated as 10% straight-line depreciation of the initial capital costs which reduce effective taxes for the first ten years. Insurance was assumed to be 1% of the total equipment costs, property taxes were based on Virginia rates. The combination of federal and state taxes were evaluated at 28%; based on current industrial tax rates. The direct fixed capital investment is split evenly into two years of building the plant, seen in Figure 9.5, where the cashflow arrows are negative. Start-up begins in the beginning of the third year, in which a gross revenue of $18.4 million will result in gross profit of $12.4 million per year. The resultant net cashflow after tax is $9.45 million during the depreciation period and $9.12 million once the plant has fully

depreciated. With a market price of $6.85 per kg of P4HB, the plant design is expected to break even 10 years after startup and yields a net present value of $55.25 million with an internal rate of return of 17.6%.

10. ENVIRONMENTAL CONCERNS

Overall, the process follows many green chemistry principles, which negates many of the environmental considerations. Implementation of green infrastructure, such as solar panels, would also be considered with design recommendations. Wastewater will be treated through filtration and activated sludge. All waste stream leaving the processes will be treated with the secondary level of treatment, as outlined in Table 8.3 of Turton et al. to ensure neutralization of any contaminants.

An ideal location would be to co-locate the plant with a source of dairy and dairy processing where the whey would be supplied at no cost with minimal transportation.

11. SAFETY CONCERNS

Oxygen is a strong oxidizer and non-flammable, but it will aid the burning of other materials. Employees handling compressed oxygen tanks will be required to complete the required OSHA training for the equipment. The facility would be considered to be at a working biosafety level of one (BSL-1), the lowest of the levels. The facility will be equipped with biohazard signs and hand and eye washing stations. All employees will be required to complete bloodborne pathogen and biosafety training as recommended by the CDC for BSL-1 operations and will be supplied with personal protective equipment, such as gloves, eye protection, and lab coats. The BSL-1 rating requires that any spills are immediate decontaminated with bleach or with an autoclave.

12. SOCIETAL IMPACT

The most successful PHA in medical applications is P4HB, due to its biodegradability, biocompatibility and mechanical properties (Le Meur et al., 2014). The large-scale production of P4HB is projected to have a positive societal impact by lowering costs of medical scaffolding for surgical patients, reducing the need for follow up surgeries, and increasing ease of surgical procedures while decreasing time of said procedures (Zheng et al., 2020).

P4HB is a high strength, resorbable polymer, used for reconstruction scaffolding for soft tissue reinforcement by multiple companies, such as Galatea Surgical. Many of the surgical products made with P4HB are designed to stimulate tissue remodeling and growth. The novel biological pathway for production of P4HB used in medical scaffolding created a more affordable and biocompatible material for human tissue reconstruction. The Surgically Shaping Children Project and the Enhancing Human Traits Project recognize that reconstructive surgery can benefit greatly from use of medical scaffolding made from biosourced, biocompatible polymers (Parens, 2006). The biocompatibility of P4HB also reduces hardship on patients by reducing the need for follow up surgeries.

Oropharyngeal cancer and oral cavity cancer may require surgeries that include reconstruction of the head, face, and neck. Scaffolding made from P4HB has been used for rhytidectomy and cosmetic breast surgery to reinforce lifted soft tissue at a much lower production cost (Williams et al., 2016). Similar P4HB surgical scaffolds made for tendon or hernia repair and for soft tissue suture is slightly elastic making it possible to apply tension for certain procedures like facial plastic surgery. P4HB can also be used to create smaller radii, strong sutures that are able to decrease the operating time by decreasing the size of

the knot bundle and reduce the knot palpability and possibility of irritation by using a soft polymer (Odermatt et al., 2012).

13. RECOMMENDATIONS AND CONCLUSIONS

This design report describes the large-scale production of medical grade polymer for surgical use such as scaffolding and sutures using genetically engineered *E. coli* at an annual rate of 2,700 tons per year. Despite the relatively low return on investment, the IRR of %17.6 for an NPV of $55.25 million suggests the investment is feasible. At this point in the design stage and economic analysis, the team recommends moving forward with the next steps in the design process. This would require obtaining quotes from vendors, investigating a real-estate location, and considering the several additional recommendations listed below. The potential benefits of additional research to lower capital investment and operating costs would likely result in a much more attractive return on investment.

Whey was chosen as the feed stock for this process, given its abundance as a waste product from the dairy processing industry. Historically expensive feedstocks, such as glucose or canola oil, presented a larger barrier to entry for producing bioplastics at a large scale due to the relative prices of feedstock and product.

Standard geometries were utilized for all bioreactors and mixing vessels of this process. While this allowed for ease of scale-up from data found in literature, it is recognized that different tank dimensions may allow for more efficient production or reduced capital costs. To further investigate this, extensive modeling and research would be necessary.

The choice of a fed-batch reactor was inspired by the results of various literature sources, in which significantly better production rates and higher resultant P4HB concentrations were apparent (Le Meur et al. 2013). Although a batch reactor would have made for a much simpler design, the fed-batch system was pursued to design the most realistic process. The choice of a linear feed rate gave the best compromise for achievable efficiency over a pulse-fed system, but it is recognized that an exponential feed rate results in the most optimal process.

Several iterations of simulation and modeling were attempted to predict the production and feasibility for the design of this process. Dynamic models utilizing Monod kinetics were used to describe the necessary feeds and resultant production of P4HB. Many of these models failed to work due to the highly complex behavior of fed-batch bioreactors. Consequently, a QSS model was chosen as the final approximation of production rate and substrate utilization. This approximation model served as a reasonable method for economic analysis but further investigation of plant design could benefit from the selection of a more accurate model.

In general, there are uncertainties associated with the fermentation modeling, pricing, and operating costs of the proposed plant. Given that the plant location is undefined, utilities are estimated via Turton, and the fermentation modeling is approximated, it is recommended that further research and experimentation are pursued. These uncertainties can be mitigated by more extensive research and would benefit most from construction of a pilot plant. More definitive economic and pricing data and supporting evidence of fermentation production via a pilot plant would yield a much higher confidence in pursing this design.

14. ACKNOWLEDGEMENTS

We would like to acknowledge Professor Anderson, our technical advisor, for all of his support and guidance throughout the course of this design project. We would like to thank Professor George Prpich as well for his invaluable help and input with designing the upstream process of this Capstone project, along with his considerate guidance. Additionally, we would like to thank Professor Giorgio Carta for providing class material to help us design the downstream process of this Capstone project and Professor Ronald Unnerstall for consulting with us regarding safety and environmental concerns associated with the plant.

15. APPENDIX A – Stream Table

Unit Operation		Stream Components:			Stream Components:		
		Stream Number	Components	Flow Rate	Stream Number	Components	Flow Rate
Wave 25 - 200 L | T = 37 C | pH = 7.0 | 48 hour cycles | 30% O2 Saturation							
IN:	Stream 1, Stream 4	**S1**	High Density Cell Cultures	1500 mL	**S4**	Growth Medium	150 L
OXYGEN SPARGING:	SO	**SO**	O2 Sparging	0.2 m^3/h			
OUT:	Stream 2	**S2**	Inoculated Cell Cultures	150 L			
Bio-Reactor - 15,000 L | T = 37 C | pH = 7.0 | rpm: 500 | 35 hour batches | 30% O2 Saturation							
IN:	Stream 2, Stream 4	**S2**	Innoculated Cell Cultures	150 L	**S4**	Growth Medium	420 L/h
OXYGEN SPARGING:	Steam O	**SO**	O2 sparging	0.2 m^3/h			
COOLING JACKET:	Stream 5, Stream 6	**S5**	Water Jacket		**S6**	Water Jacket	
OUT:	Stream 7	**S7**	Cell Broth	1350 L			
Rotating Disc Centrifuge - Rotational Speed = 3000 RPM | 50 Discs | Bowl Diameter = 24" | Disc Angle = 45 | Disc Length = 1m							
IN:	Stream 7	**S7**	Cell Broth	3750 L/h			
OUT:	Stream 10, Stream 9	**S10**	P4HB Pellet	405 L/h	**S9**	Waste Cell Medium	3346 L/h
Homogenizer - Pressure = 15,000 psi							
IN:	Stream 10	**S10**	P4HB Pellet	405 L/h			
OUT:	Stream 11	**S11**	Homogenized P4HB Mixture	405 L/h			
Stir Tanks - Aggitation Speed = 500 RPM | Retention time for Stir Tank 2 = 1 hour | 24 hours for tanks 1 and 3							
Stir Tank 1 IN:	Stream 3	**S3**	Growth Medium Mixing	**			
Stir Tank 1 OUT:	Stream 4	**S4**	Growth Medium	420 L/h			
Stir Tank 2 IN:	Stream 12	**S12**	Liquid Activated Charcoal Mixing	**			
Stir Tank 2 OUT:	Stream 13	**S13**	Liquid Activated Charcoal	329 L/h			
Stir Tank 3 IN:	Stream 11, Stream 13	**S11**	Homogenized P4HB Mixture	405 L/h	**S13**	Liquid Activated Charcoal	329 L/h
Stir Tank 3 OUT:	Stream 14	**S14**	Charcoal and P4HB Slurry	734 L/h			
Rotary Filtration System - 0.45 mm Membranes | Metallic Lace Tissue | 100 mBar							
IN:	Stream 14	**S14**	Charcoal and P4HB Slurry	734 L/h			
OUT:	Stream 15, Stream 6	**S15**	Waste	409 L/h	**S16**	Filtered Slurry	396 L/h
Rotary Drier - T = 45 C | Pressure = 200 mBar | 12 hour dry time							
IN:	Stream 16	**S16**	Filtered Slurry	78585 kg			
Air Jacket:	Stream 17, Stream 18	**S17**	Air		**S18**	Air	
OUT:	Stream 19	**S19**	Drier P4HB Mix	71441 kg			
Vacuum Drier - T = 45 C | Pressure = 100 mBar | 24 hour dry time							
IN:	Stream 19	**S19**	Drier P4HB Mix	71441 kg			
OUT:	Stream 20	**S20**	Driest P4HB Mix	68039 kg			
Blown Film Extruder - T = 135 C | Film Width = 240" | Film Thickness = 200 microns | Screw Size = 45mm							
IN:	Stream 20	**S20**	Driest P4HB Mixture	68039 kg			
OUT:	Stream 21	**S21**	Rolled P4HB Sheets	68039 kg			

Figure A: Stream Table - Corresponding flow rates and batch size for the process flow diagram shown in section 4

16. APPENDIX B- NOMENCLATURE

Variable	Name	Units
μ	Specific growth rate	1/hr
μ_{max}	Maximum specific growth rate	1/hr
F	Volumetric feed rate into bioreactor	L/hr
D	Dilution rate	1/hr
K_s	Substrate constant of saturation	g/L
X	Cell mass density	g CDW/L
X^t	Total cell mass	g cells
V	Volume of the system	L or m^3
S	Concentration of substrate	g substrate/L
S^t	Total mass of substrate	g substrate
P	Concentration of polymer product	g product/L
P^t	Total mass of the polymer product	g product
Y_{XS}	Yield coefficient of the substrate to mass yield	g CDW/g Substrate
Y_{PX}	Yield coefficient for cell mass to product	g CDW /g product
Y_{PS}	Yield Coefficient of Substrate to Product	g product /g substrate
$Q_{O2,max}$	Oxygen utilization rate per cell mass	g O_2/ (gCDW/L * hr)
OUR_{max}	Oxygen uptake rate	g O_2/ hr
H_t	Tank height	m
D_t	Tank diameter	m
D_i	Impeller diameter and spacing	m
H_l	Height of the liquid level	m
V_T	Tank volume	m^3
A_T	Tank Area	m^2
n_i	Number of impellers	(impellers)
$k_{La,O2}$	Volumetric mass transfer coefficient	1/h
N or N_{stir}	Impeller rotational speed	rev/s or RPM
ω	Rotational speed	rad/s
VVM or Q_g	Volume gas feed rate per tank volume or	vol/(vol min) or m^3/s

	Volumetric flow rate of oxygen	
K_{la}	Volumetric mass transfer rate	s/m^3
v_s	Superficial gas velocity	m/s
φ	Hold up or volume change due to aeration	[unitless]
ρ_L	Liquid density	kg/m^3
μ_L or η	Liquid viscosity	Pa-s
P	Power of ungassed system	W
P_g	Power corrected for gassed system	W
Re	Reynolds Number	[unitless]
N_P	Power Number	[unitless]
N_A	Aeration Number	[unitless]
P/P_g	Gassing Factor	[unitless]
P_g/V	Specific power input of the gassed system	W/m^3
P_m	Specific mass power input of gassed system	W/kg
r_p	Radius of a particle for centrifuge	mm
ρ_p	Density of *E. coli* and polymer	kg/m^3
V_g	Sedimentation velocity for centrifuge unit	cm/hr
$P_{H,}$	Hydraulic power	W
v	Fluid velocity through the filtration unit	m/s
ΔP	Applied Pressure for filtration	Pa
R	Flow resistance parameter for filtration	m^{-1}
R_m	Filter medium resistance	m^{-1}
R_c	Filter cake resistance	m^{-1}
L	Filter cake thickness as a function of time	m
α	Filter cake resistance parameter	m^{-2}
V_b	Suspension volume for filtration unit	m^3
V	Accumulated volume of filtrate	m^3
Q	Filtrate flow rate	m^3/s

C	Slurry concentration to filtration unit	kg solid particle /m^3
ρ_c	Filter cake density of	kg solid/m^3
A	Filter cake area	m^2
Q_y	Minimum heat supply rate for vaporization of water in the dryer	J
$C_{P,\ P4HB}$	Heat of vaporization of	J/kg*K
Q_{in}	The heat supply rate for the dryer	W
BUR	Extruder blow up ratio	[unitless]
DDR	Draw-down ratio	[unitless]
BR	Blow ratio	[unitless]
LFW	Lay flat width	[unitless]
D_D	Die diameter for extruder	m
D_B	Bubble diameter for extruder	m
Q_P	Flowrate for fluid in a pump	m^3/s
dP	Total pressure differential a pump	Pa
ΔP	The pressure difference between source and destination of pumps	Pa
f_L	Pressure drop due to frictional losses for a pump	Pa
H_g	Hydrostatic or gravity head	Pa

17. WORKS CITED

Amaro, T. M. M. M., Rosa, D., Comi, G., & Iacumin, L. (2019). Prospects for the Use of Whey for Polyhydroxyalkanoate (PHA) Production. *Frontiers in Microbiology*, *10*. https://doi.org/10.3389/fmicb.2019.00992

C. Reddy, R Ghai, V. Rashmi, & C. Kalia. (2003). Polyhydroxyalkanoates: An overview. *Biores. Technology*, 137–146.

Centers for Disease Control and Prevention. (2019, April 4). *Ethylene Oxide Sterilization | Disinfection & Sterilization Guidelines | Guidelines Library | Infection Control |CDC*. https://www.cdc.gov/infectioncontrol/guidelines/disinfection/sterilization/ethylene-oxide.html

Don W. Green & Robert H. Perry. (2008). *Perry's Chemical Engineering Handbook* (8th ed.). McGraw-Hill. DOI:10.1036/0071422943

Electric Power Monthly—U.S. Energy Information Administration (EIA). (n.d.). Retrieved May 11, 2021, from https://www.eia.gov/electricity/monthly/epm_table_grapher.php

Hagstrum, D. (2016). *Fundamentals of Stored-Product Entomology*. Elsevier.

Le Meur, S., Zinn, M., Egli, T., Thöny-Meyer, L., & Ren, Q. (2013). Poly(4-hydroxybutyrate) (P4HB) production in recombinant Escherichia coli: P4HB synthesis is uncoupled with cell growth. *Microbial Cell Factories*, *12*(1), 123. https://doi.org/10.1186/1475-2859-12-123

Le Meur, S., Zinn, M., Egli, T., Thöny-Meyer, L., & Ren, Q. (2014). Improved productivity of poly (4-hydroxybutyrate) (P4HB) in recombinant Escherichia coli using glycerol as

the growth substrate with fed-batch culture. *Microbial Cell Factories*, *13*(1), 131. https://doi.org/10.1186/s12934-014-0131-2

Lin, Z., Zhang, Y., Yuan, Q., Liu, Q., Li, Y., Wang, Z., Ma, H., Chen, T., & Zhao, X. (2015). Metabolic engineering of Escherichia coli for poly(3-hydroxybutyrate) production viathreonine bypass. *Microbial Cell Factories*, *14*(1), 185. https://doi.org/10.1186/s12934-015-0369-3

Martin, D. P., & Williams, S. F. (2003). Medical applications of poly-4-hydroxybutyrate: A strong flexible absorbable biomaterial. *Biochemical Engineering Journal*, *16*(2), 97–105. https://doi.org/10.1016/S1369-703X(03)00040-8

Misra, S., Srivastava, A. K., Raghuwanshi, S., Sharma, V., & Bisen, P. (2018). Medical grade biodegradable polymers: A perspective from gram-positive bacteria. In *Fundamental Biomaterials: Polymers* (pp. 267–286). https://doi.org/10.1016/B978-0-08-102194-1.00012-8

Odermatt, E. K., Funk, L., Bargon, R., Martin, D. P., Rizk, S., & Williams, S. F. (2012). MonoMax Suture: A New Long-Term Absorbable Monofilament Suture Made from Poly-4-Hydroxybutyrate. *International Journal of Polymer Science*, *2012*, 1–12. https://doi.org/10.1155/2012/216137

Parens, E. (Ed.). (2006). *Surgically shaping children: Technology, ethics, and the pursuit of normality*. Johns Hopkins University Press.

Peters, M., Timmerhaus, K., & West, R. (2003). *Plant design and economics for chemical engineers* (Fifth). McGraw-Hill Higher Education.

Petrides, D., Carmichael, D., Siletti, C., & Koulouris, A. (2014). Biopharmaceutical Process Optimization with Simulation and Scheduling Tools. *Bioengineering (Basel)*, *Bioengineering*. https://doi.org/10.3390/bioengineering1040154

Reis, M., Serafim, L., & Freitas, M. (2013). Bioconversion of cheese whey into polyhydroxyalkanoates. *Joana Oliveira Pais*.

Ricardo, L., Vieira, G., de, A., & Olzany, S. (2000). Fermentation of sweet whey by recombinant Escherichia coli KO11. *Brazilian Journal of Microbiology*, *31*. https://doi.org/10.1590/S1517-83822000000300011

Turton, R., Baille, B., Whiting, W., & Shaelwitz, J. (2009). *Analysis, synthesis, and design of chemical processes* (3rd ed.). Prentice Hall International Series in the Physical and Chemical Sciences.

U.S. Department of Health and Human Services. (2015). Analytical Procedures and Methods Of Validation for Drugs and Biologics. Guidance for Industry. *Food and Drug Administration*. https://www.usp.org/

Utsunomia, C., Ren, Q., & Zinn, M. (2020). Poly(4-Hydroxybutyrate): Current State and Perspectives. *Frontiers in Bioengineering and Biotechnology*, *8*. https://doi.org/10.3389/fbioe.2020.00257

Viitanen, M. I., Vasala, A., Neubauer, P., & Alatossava, T. (2003). Cheese whey-induced high-cell-density production of recombinant proteins in Escherichia coli. *Microbial Cell Factories*, *2*, 2. https://doi.org/10.1186/1475-2859-2-2

Vlachopoulos, J., Castillo, R., Polychronopoulos, N., & Tanifuji, Shin-Ichiro. (2012). *Blown Film Dies* (pp. 141–168).

Wagner, J. R., Mount, E. M., & Giles, H. F. (2014a). 14—Processing Conditions. In J. R. Wagner, E. M. Mount, & H. F. Giles (Eds.), *Extrusion (Second Edition)* (pp. 181–192). William Andrew Publishing. https://doi.org/10.1016/B978-1-4377-3481-2.00014-4

Wagner, J. R., Mount, E. M., & Giles, H. F. (2014b). 46—Blown Film. In J. R. Wagner, E. M. Mount, & H. F. Giles (Eds.), *Extrusion (Second Edition)* (pp. 539–549). William Andrew Publishing. https://doi.org/10.1016/B978-1-4377-3481-2.00046-6

Wampfler, B., Ramsauer, T., Kehl, K., Zinn, M., & Thöny-Meyer, L. (2010). Application of activated charcoal in the downstream processing of bacterial olefinic poly(3-hydroxyalkanoates). *Chimia*, *64*(11), 784–788. https://doi.org/10.2533/chimia.2010.784

Williams, S. F., Martin, D. P., & Moses, A. C. (2016). The History of GalaFLEX P4HB Scaffold. *Aesthetic Surgery Journal*, *36*(Suppl 2), S33–S42. https://doi.org/10.1093/asj/sjw141

Zheng, Y., Chen, J.-C., Ma, Y.-M., & Chen, G.-Q. (2020). Engineering biosynthesis of polyhydroxyalkanoates (PHA) for diversity and cost reduction. *Metabolic Engineering*, *58*, 82–93. https://doi.org/10.1016/j.ymben.2019.07.004

Zhou, X.-Y., Yuan, X.-X., Shi, Z.-Y., Meng, D.-C., Jiang, W.-J., Wu, L.-P., Chen, J.-C., & Chen, G.-Q. (2012). Hyperproduction of poly(4-hydroxybutyrate) from glucose by recombinant Escherichia coli. *Microbial Cell Factories*, *11*(1), 54. https://doi.org/10.1186/1475-2859-11-54